# Acyl chain asymmetry and polyunsaturation of brain phospholipids facilitate membrane vesiculation without leakage

Marco M. Manni*, Marion L. Tiberti*, Sophie Pagnotta†, Hélène Barelli*, Romain Gautier* and Bruno Antonny*‡

*Institut de Pharmacologie Moléculaire et Cellulaire, Université Côte d'Azur et CNRS, 660 Route des Lucioles, 06560 Valbonne, France

†Centre Commun de Microscopie Appliquée, Université Côte d'Azur, Parc Valrose, Nice

‡corresponding author. B Antonny, IPMC CNRS, 660 route des lucioles, 06560 Valbonne-Sophia Antipolis, France. Tel: 33 4 93 95 77 75, antonny@ipmc.cnrs.fr

Keywords: Polyunsaturated phospholipids, membrane curvature, membrane fission, membrane permeability, Dynamin, BAR domain

**Abstract**

Phospholipid membranes form cellular barriers but need to be flexible enough to divide by fission. Phospholipids generally contain a saturated fatty acid (FA) at position *sn1* whereas the *sn2*-FA is saturated, monounsaturated or polyunsaturated. Our understanding of the impact of phospholipid unsaturation on membrane flexibility and fission is fragmentary. Here, we provide a comprehensive view of the effects of the FA profile of phospholipids on membrane vesiculation by dynamin and endophilin. Coupled to simulations, this analysis indicates that: (i) phospholipids with two polyunsaturated FAs make membranes prone to vesiculation but highly permeable; (ii) asymmetric *sn1*-saturated-*sn2*-polyunsaturated phospholipids provide a tradeoff between efficient membrane vesiculation and low membrane permeability; (iii) When incorporated into phospholipids, docosahexaenoic acid (DHA; omega-3) makes membranes more deformable than arachidonic acid (omega-6). These results suggest an explanation for the abundance of *sn1*-saturated-*sn2*-DHA phospholipids in synaptic membranes and for the importance of the omega-6/omega-3 ratio on neuronal functions.

**Keywords**

Polyunsaturated phospholipid, omega-6, omega-3, membrane deformation, membrane fission, dynamin, BAR domain

## Introduction

Although it is common knowledge that polyunsaturated fatty acids (PUFAs) especially omega-3 FAs are important for health, the underlying mechanisms are not fully understood (Bazinet and Layé, 2014; Marszalek and Lodish, 2005; Stillwell and Wassall, 2003). PUFAs act through three different states: as free molecules, as precursors of biological mediators, or as esters in membrane phospholipids. The third form results from the activity of acyl transferases, which selectively incorporate defined fatty acids into phospholipids (Harayama et al., 2014; Shindou et al., 2013). This allows cells to control the acyl chain profile of their phospholipids, which varies tremendously among organisms, tissues and cells, and even among organelles (Harayama et al., 2014; Hulbert, 2003; Shindou et al., 2013). Interestingly, the FA diversity in phospholipids applies mostly to the *sn2* position of the glycerol backbone, hence resulting in asymmetric phospholipids containing a saturated FA at position *sn1* and an unsaturated FA at position *sn2* (Hanahan et al., 1960; Lands, 1963; Tattrie, 1959; Yabuuchi and O'Brien, 1968).

For example, the brain is enriched in phospholipids with PUFAs, notably in the case of phosphatidylethanolamine (PE) and phosphatidylserine (PS) (Tam and Innis, 2006; Yabuuchi and O'Brien, 1968). Moreover, an interesting pattern has been detected in neurons, where the axon tip is enriched in phosphatidylcholine (PC) molecules containing arachidonate (AA or 20:4 omega-6) or docosahexaenoate (DHA or 22:6 omega-3) at the expense of less unsaturated PC species (Yang et al., 2012). Thus, phospholipids with PUFAs are found at very high concentration in synaptic vesicles, where they account for up to 70 mol% of the phospholipid pool (Takamori et al., 2006). Retinal discs also show very high concentrations of phospholipids containing PUFAs (Boesze-Battaglia and Schimmel, 1997; Rice et al., 2015). These striking enrichments suggest that the fatty acyl chain profile of phospholipids could impact on the properties of cellular membranes.

We previously showed that phospholipids with the *sn2* PUFA DHA facilitate the membrane shaping and fission activities of dynamin and endophilin (Pinot et al., 2014). These proteins are involved in the formation of endocytic vesicles by assembling into spirals around the neck of membrane buds (Antonny et al., 2016; Boucrot et al., 2015; Farsad et al., 2001; Slepnev and De Camilli, 2000; Sundborger et al., 2011). Physical manipulations, molecular dynamics simulations and biochemical measurements revealed that DHA-containing phospholipids decrease membrane-bending rigidity by adapting their conformation to membrane curvature, hence providing an advantage for membrane deformation and fission by the dynamin endophilin complex (Pinot et al., 2014) in contrast to more rigid membranes, which are less prone to fission (Morlot et al., 2012). More generally, the flexibility of polyunsaturated phospholipids along the membrane normal (*z* direction) might soften various mechanical stresses in the membrane (Barelli and Antonny, 2016).

The activity of dynamin and endophilin was previously determined on extreme membrane compositions: the phospholipids were either saturated-monounsaturated (16:0-18:1) or saturated-DHA (18:0-22:6?3) (Pinot et al., 2014). However, others PUFAs are found in phospholipids (Harayama et al., 2014; Tam and Innis, 2006; Yabuuchi and O'Brien, 1968). The most common are 18:2 omega-6 (linoleate), 18:3 omega-3 (linolenate), and 20:4 omega-6 (arachidonate), which differ by the number of double bonds and their position along the chain (Fig. 1A). Here, we present a comprehensive study of the impact of phospholipid unsaturation on the mechanical activities of dynamin and endophilin where we varied both the degree of FA unsaturation and the combination of FAs at position *sn1* and *sn2* of phospholipids considering that most natural phospholipids have an asymmetric FA distribution (Hanahan et al., 1960; Lands, 1963; Tattrie, 1959; Yabuuchi and O'Brien, 1968). The analysis reveals that the combination of an *sn1* saturated acyl chain and an *sn2* polyunsaturated acyl chain solves the conundrum between making a membrane very permissive to vesiculation while maintaining a proper control of membrane permeability.

## RESULTS

### *Comprehensive analysis of the effect of phospholipid unsaturation on dynamin GTPase activity*

GTP hydrolysis in the dynamin spiral occurs by a mutual nucleophilic attack between dynamin molecules from adjacent rungs (Chappie et al., 2011). Consequently, the rate of GTP hydrolysis depends on dynamin self-assembly and, in effect, increases from negligible values in solution where dynamin is not polymerized, to rates in the range of 2 to 5 s-1 on optimal membrane templates where dynamin forms spirals (Stowell et al., 1999). We reasoned that GTPase measurements should provide a robust, although indirect, assay to survey a comprehensive library of liposomes made of phospholipids of defined acyl chains for their permissibility to the mechanical activity of dynamin. Dynamin was purified from rat brain, which contains mostly the neuron-specific dynamin-1 isoform, which has a higher membrane curvature generating activity than dynamin-2, the ubiquitous isoform (Liu et al., 2011). This screen could also be performed in the presence of proteins that cooperate with dynamin (e.g. BAR domains). Thereafter, the most interesting membrane parameters could be further analyzed by more direct assays of dynamin mechanical activity (e.g. EM observations or assays with Giant Unilamellar Vesicles (GUVs)), which are difficult to standardize for large screens. This second round of analysis is important because conditions exist where dynamin readily self-assembles and undergoes fast GTP hydrolysis and yet does not efficiently promote membrane vesiculation (Neumann and Schmid, 2013; Stowell et al., 1999).

We prepared large unilamellar vesicles (extrusion 400 nm) made of five lipids: PC, PE, PS, phosphatidylinositol(4,5)bisphosphate (PI(4,5)$P_2$) and cholesterol (**Figure 1A**). The relative amount of these lipids was kept constant and was chosen to be compatible with the recruitment of both dynamin, which interacts with PI(4,5)$P_2$, and of BAR domain proteins, which interacts with negatively charged lipids (e.g. PS and PI(4,5)$P_2$). However, PI(4,5)$P_2$ was present at low density (1 mol %; close to physiological values) to amplify the need for other facilitating factors such as cooperation with endophilin and membrane flexibility. The only variable in the liposome formation was the acyl chain profile of PC, PE and PS, which accounted for 99% of total phospholipids. Using commercially available or custom lipids, we systematically changed the acyl chain profile in two ways (**Supplementary File Table S1** and **Figure 1A**). First, we gradually increased the length and unsaturation level of both the *sn1* and *sn2* acyl chains of PC, PE and PS according to the series 14:0-14:0, 18:1-18:1 (omega-9), 18:2-18:2 (omega-6), 20:4-20:4 (omega-6), and 22:6-22:6 (omega-3). Considering that most physiological phospholipids have different acyl chains at positions *sn1* and *sn2* (Hanahan et al., 1960; Lands, 1963; Tattrie, 1959; Yabuuchi and O'Brien, 1968), we performed a second series in which we maintained a saturated (18:0) acyl chain at position *sn1* and solely changed the *sn2* chain (18:0-18:1, 18:0-18:2, 18:0-20:4, 18:0-22:6). These asymmetric combinations are most frequent in mammalian lipids. The parallel increase in acyl chain length and unsaturation enabled all lipid mixtures to be fluid above 20°C (Huang, 2001).

108 The result of this comprehensive analysis is shown in Figure 1B (typical GTPase experiments are provided in
109 **Figure 1-figure supplement 1A**). Despite the identical composition of all liposomes in term of lipid polar
110 head groups, the rate of GTP hydrolysis by dynamin varied up to 300-fold indicating that dynamin is very
111 sensitive to the acyl chain content of the lipid membrane on which it acts. Two parameters emerged: acyl
112 chain asymmetry and acyl chain unsaturation. First, the GTPase activity of dynamin increased dramatically
113 (x 20) on membranes made of symmetric diunsaturated phospholipids compared to asymmetric saturated-
114 unsaturated phospholipids. Second, the GTPase activity of dynamin increased with the unsaturated level of
115 phospholipids (18:1 < 18:2 < 20:4 < 22:6), a trend that was observed in both symmetric and asymmetric
116 phospholipid series.

117 ***Membranes with symmetric polyunsaturated phospholipids are highly permeable to solutes***

118 How to explain the spectacular effect of symmetric diunsaturated phospholipids on the GTPase activity of
119 dynamin? By negative staining electron microscopy, we observed that dynamin alone extensively deformed
120 22:6-22:6 liposomes, whereas 18:0-22:6 liposomes were largely unaffected (**Figure 1C and Figure 1-figure**
121 **supplement 1B**). The analysis was performed either in the presence of GTPγS, where dynamin self-
122 assembles into stable spirals on membranes, or in the presence of GTP, where dynamin spirals further
123 constrict to promote liposome vesiculation into round profiles of ≈ 20 nm in diameter. Liposomes
124 containing phospholipids with two polyunsaturated acyl chains appeared exceptionally malleable as
125 compared to liposomes made of phospholipids with one saturated and one polyunsatured acyl chain.

126 Deformation of spherical liposomes is necessarily accompanied by a diminution of volume of the
127 encapsulated solution. For example, the COPI coat is more efficient at making vesicles from liposomes that
128 have been permeabilized with a pore-forming toxin (Manneville et al., 2008). Because a previous study
129 reported that membranes made of 18:2-18:2-PC or 18:3-18:3 PC showed a two to three fold higher water
130 permeability than membranes made of 18:0-18:1-PC or 18:0-18:2-PC (Olbrich et al., 2000), we suspected
131 that membranes with dipolyunsaturated phospholipids might be very permissive to deformation by
132 dynamin due to higher permeability.

133 To assess the permeability of our artificial membranes, we combined molecular dynamics simulations with
134 various measurements. The simulations were performed at the all-atom scale on bilayers containing 2 x 144
135 phospholipids with the same composition as that used in the experiments. To evaluate water permeability,
136 we determined the number of water molecules that visit the hydrophobic part of the membrane during a
137 period of 100 ns (**Figure 2A**). These movements were subdivided into two classes: events in which the water
138 molecule fully crosses the lipid bilayer; events in which the water molecule enters into the hydrophobic
139 region of the bilayer and then exists on the same side. In saturated (14:0-14:0) membranes, only few water
140 movements were detected. In membranes made of phospholipids with one unsaturated FA, the number of

141 moving water molecules increased up to 10-fold with the level of acyl chain unsaturation (18:1 < 18:2 < 20:4
142 < 22:6) (**Figure 2A**). Importantly, membranes with phospholipids containing two unsaturated FA showed a
143 further 2 to 3-fold increase in the number of moving water molecules as compared to membranes with
144 asymmetric saturated-unsaturated phospholipids. This increase occurred whatever the acyl chain
145 considered (e.g. 20:4-20:4 *vs* 18:0-20:4 or 22:6-22:6 *vs* 18:0-22:6).

146 If membranes with symmetric polyunsaturated phospholipids are more hydrated than membranes with
147 asymmetric saturated-unsaturated phospholipids, this should influence the fluorescence of polarity-
148 sensitive dyes at the membrane interface. To investigate this possibility, we used a recently synthesized
149 push-pull pyrene (PA). This probe, similarly to the popular probe Laurdan, changes its emission maximum as
150 a function of membrane hydration and solvent relaxation, which are parameters linked to lipid order (Niko
151 et al., 2016). PA showed a gradual red shift in emission when the number of double bonds in the *sn2* acyl
152 chain increased (18:0-18:1 < 18:0-18:2 < 18:0-20:4 < 18:0-22:6) (**Figure 2B and Figure 2-figure supplement**
153 **1**). However, replacing asymmetric saturated-polyunsaturated phospholipids with dipolyunsaturated
154 phospholipids caused a much larger red shift (**Figure 2B and Figure 2-figure supplement 1**; e.g. 18:0-22:6 <<
155 22:6-22:6), suggesting that duplication of the PUFA in phospholipids dramatically increased membrane
156 hydration.

157 Considering the importance of maintaining ion gradients across biological membranes, we next assessed
158 the permeability of our liposomes to the oxoanion dithionite ($[S_2O_4]^{2-}$) by an NBD quenching assay. When
159 added to liposomes, dithionite (MW = 128 Da) immediately quenches the fraction of (C16:0-C16:0) PE-NBD
160 that is present in the outer leaflet. This fraction is about 50 % but varies depending on factors like
161 membrane curvature or the presence of multi-lamellar liposomes (Kamal et al, 2009). Thereafter, dithionite
162 slowly quenches the remaining PE-NBD molecules. This process occurs either by penetration of dithionite
163 into the liposomes or because of PE-NBD flip-flop. Previous work established that dithionite entry is about
164 1000 times faster than lipid flip-flop (Armstrong et al, 2003). Therefore, the slow phase in PE-NBD
165 quenching experiments should reflect dithionite permeability. **Figure 2C** shows that membrane
166 permeability to dithionite modestly increased with the level of polyunsaturation in asymmetric
167 phospholipids (18:0-18:1 < 18:0-18:2 < 18:0-20:4 < 18:0-22:6) and that liposomes with symmetric
168 polyunsaturated phospholipids showed a > 10-fold higher permeability. This effect was particularly evident
169 for 20:4-20:4 and 22:6-22:6 membranes: 95% of PE-NBD was quenched after 300 s incubation with
170 dithionite as compared to 55-60 % in the case of 20:4 and 18:0-22:6 membranes. Note that the liposomes
171 used in the dithionite experiments were the same as that used in the dynamin experiments (see Figure 1B)
172 to allow a direct comparison between the two assays. However, a drawback of liposomes obtained by
173 extrusion through large pore size filters (here 400 nm), is the presence of multi-lamellar species (Kamal et
174 al, 2009). For such species, dithionite has to cross several bilayers to fully quench all PE-NBD molecules. This
175 effect probably explains why the second phase of PE-NBD quenching, although quite fast in the case of

176 20:4-20:4 and 22:6-22:6 liposomes, was not complete; a small percentage (≈ 5 %) of NBD signal remained
177 unquenched after 300 s incubation (**Figure 2C**). Despite these limitations, these experiments suggest that
178 the presence of two polyunsaturated acyl chains in phospholipids strongly compromise membrane
179 impermeability to ions.

180 Last, we visualized the permeability of GUVs to the large fluorescent solute Alexa A488 maleimide (MW =
181 720 Da). This compound was added externally to the GUVs, which were imaged by fluorescence microscopy
182 (**Figure 2D**). Again, the difference between symmetric and asymmetric polyunsaturated phospholipids was
183 clear-cut. GUVs containing 55 mol% 22:6-22:6 phospholipids were about 10 times more permeable to Alexa
184 A488 maleimide than GUVs containing 55 mol% 18:0-22:6 phospholipids.

185 Altogether, these experiments revealed a remarkable correlation between the ability of dynamin alone to
186 readily vesiculate membranes and the permeability of these membranes to water and even to large or
187 charged solutes.

188 ***Dynamin GTPase activity on asymmetric saturated-polyunsaturated phospholipids***

189 If membranes with symmetric diunsaturated phospholipids appear exceptionally prone to vesiculation by
190 dynamin, their high permeability to ions and large solutes disqualify them for the formation of selective
191 membrane barriers. The GTPase assay of **Figure 1B** and the membrane permeability experiments of **Figure 2**
192 suggest that asymmetric saturated-polyunsaturated phospholipids offer a compromise between low
193 permeability and dynamin activity. Even though the intrinsic GTPase activity of dynamin on such liposomes
194 was low, it increased about 10 times in the presence endophilin-A1 (**Figure 1B**).

195 In cells, endophilin works in close partnership with dynamin both through protein/protein interactions and
196 through the ability of the two proteins to form membrane-deforming spirals (Boucrot et al., 2015; Farsad et
197 al., 2001; Sundborger et al., 2011). The BAR domain of endophilin is followed by an SH3 domain, which
198 interacts with the proline-rich region of dynamin leading to cooperative BAR/dynamin membrane
199 recruitment(Farsad et al., 2001; Meinecke et al., 2013; Sundborger et al., 2011). In addition, membrane
200 deformation by BAR domains facilitates dynamin self-assembly, which by itself is a relatively weak
201 membrane deforming protein and which preferentially self-assembles on pre-curved membranes
202 (Neumann and Schmid, 2013; Roux et al., 2010), unless the membranes are particularly deformable as
203 observed with symmetric unsaturated phospholipids (**Figure 1C**).

204 These considerations and the fact that asymmetric polyunsaturated phospholipids are much more frequent
205 than symmetric ones in biological membranes prompted us to focus on reconstitutions in which both
206 dynamin and endophilin were present and acted on membranes with asymmetric phospholipids. Under
207 such conditions, the exact nature of the *sn2* acyl chain appeared very important: significant differences in

208 the dynamin GTPase activity were observed between acyl chain combinations that are chemically very close
209 (e.g. 18:0-20:4 *vs* 18:0-22:6) (**Figure 1A**).

210 To better analyze these differences, we repeated the GTPase assay under conditions where we gradually
211 increased the amount of asymmetric polyunsaturated phospholipids at the expense of 18:0-18:1
212 phospholipids (**Figure 3**). Two omega-3 combinations (18:0-18:3 and 18:0-22:6) and two omega-6
213 combinations (18:0-18:2 and 18:0-20:4) were included in the analysis to evaluate the importance of the
214 double bond position. All polyunsaturated phospholipids facilitate dynamin GTPase activity. However, the
215 effect of 18:0-22:6 phospholipids surpassed by 2 to 4-fold that observed with the less complex asymmetric
216 polyunsaturated phospholipids (18:0-18:2, 18:0-18:3 and 18:0-20:4) (**Figure 3**). Dynamin GTPase activity
217 plateau at about 60 mol% of 18:0-22:6 phospholipids, close to the amount of polyunsaturated lipids in
218 synaptic vesicles (Takamori et al., 2006).

219 To check that the effect of asymmetric polyunsaturated phospholipids was not restricted to our particular
220 conditions, we modified several parameters. First, we varied the % of PI(4,5)$P_2$. In a background of 18:0-
221 18:1 phospholipids, the GTPase activity of dynamin in the presence of endophilin was low and increased
222 with the % of PI(4,5)$P_2$ (from 0 to 5 %; **Figure 3-figure supplement 1A**). In a background of 18:0-18:2, 18:0-
223 18:3 or 18:0-20:4 phospholipids, the GTPase activity was much higher and required not more than 1 mol%
224 PI(4,5)$P_2$. Strikingly, the activity of dynamin was almost maximal with 18:0-22:6 phospholipids even in the
225 absence of PI(4,5)$P_2$ (**Figure 3-figure supplement 1A**). Next, we replaced endophilin by SNX9, another BAR-
226 domain containing protein that interacts with dynamin. Both endophilin and SNX9 increased dynamin
227 activity much more efficiently on membranes containing 18:0-22:6 phospholipids or 18:0-20:4 than 18:0-
228 18:1 phospholipids (**Figure 3-figure supplement 1B**). In addition, SNX9 was more efficient than endophilin
229 for assisting dynamin activity in agreement with a previous study (Neumann and Schmid, 2013). All these
230 experiments converge towards the same conclusions. First, all asymmetric saturated-polyunsaturated
231 phospholipids favor dynamin GTPase activity, notably under conditions close to physiological conditions
232 (low concentration of PI(4,5)$P_2$, low protein concentration, cooperation with BAR-domain proteins). Second,
233 docosahexaenoic acid (22:6), which is the most polyunsaturated species of the omega-3 family, surpasses
234 all other tested species including arachidonate (20:4), the most polyunsaturated species of the omega-6
235 family.

236 ***Membrane fission by dynamin and endophilin is sensitive to the omega-6/omega-3 ratio***

237 18:0-20:4 and 18:0-22:6 phospholipids are abundant in specialized membranes (e.g. synaptic vesicles;
238 Takamori et al., 2006). Considering the importance of the omega-6/omega-3 ratio for health, we next
239 focused on these acyl chain combinations and used 18:0-18:1 membranes as negative control.

240 By transmission electron microscopy (TEM) we observed that both 18:0-20:4 and 18:0-22:6 liposomes but
241 not 18:0-18:1 liposomes, became extensively deformed after incubation with dynamin, endophilin and
242 GTPγS or GTP. With GTPγS, membrane tubulation dominated (**Figure 4A**). The tubes were surrounded by a
243 protein spiral with a pitch of ~ 20 nm characteristic of the endophilin-dynamin complex (Farsad et al., 2001;
244 Pinot et al., 2014; Sundborger et al., 2011) (Figure 4B and Figure 4-figure supplement 1A). However, the
245 tubes formed from 18:0-22:6 membranes were significantly thinner than the tubes formed from 18:0-20:4
246 membranes (**Figure 4B**). With GTP present, liposome vesiculation dominated (Figure 4A). The size
247 distribution of the membrane profiles was different between 18:0-20:4 and 18:0-22:6 phospholipids (**Figure**
248 **4C**). With 18:0-20:4 phospholipids, there was a remaining peak of large membrane profiles (R > 50 nm),
249 which coexisted with a peak of small vesicles (R < 50 nm). With 18:0-22:6 phospholipids, the liposomes
250 were almost fully transformed into small vesicles. In addition, the vesicles formed from 18:0-22:6
251 membranes were slightly smaller than that formed from 18:0-20:4 membranes (**Figure 4C**). Note that after
252 short incubation with GTP, some tubes were observed both with 18:0-20:4 and 18:0-22:6 liposomes (Figure
253 4-figure supplement 1B). These tubes were not straight as with GTPγS but showed constrictions, suggesting
254 snapshots in the process of membrane fission (black arrows in **Figure 4-figure supplement 1B**)

255 Considering the technical limitations caused by spontaneous membrane fission on TEM grids (Danino,
256 Moon, and Hinshaw, 2004), we next performed a GUV shrinking assay (Meinecke et al., 2013). In these
257 experiments, dynamin, endophilin and GTP were added to GUVs containing 55 mol% of polyunsaturated
258 phospholipids, which were pre-stabilized in buffer at the reaction temperature (37 °C). Dynamin, endophilin
259 and GTP caused GUV consumption over time for both 18:0-20:4 and 18:0-22:6 membranes (**Figure 5A**) but
260 not for the control GUVs that contained only 18:0-18:1 phospholipids (**Figure 5-figure supplement 1A and**
261 **B**). After 1h of incubation, the difference between 18:0-20:4 and 18:0 22:6 phospholipids was significant, as
262 we detected a larger population of shrunk 18:0-22:6 GUVs and a higher amount of intact 18:0-20:4 GUVs
263 (**Figure 5B**). The difference in GUV shrinking between 18:0-20:4 and 18:0-22:6 phospholipids was already
264 evident after 15 min and increased over time (**Figure 5C**).

265 ***Differences between asymmetric polyunsaturated phospholipids as captured by MD simulations***

266 To better understand the advantage provided by asymmetric polyunsaturated phospholipids on membrane
267 deformation and fission, we conducted MD simulations on lipid bilayers. In the coarse-grained mode, we
268 considered large membrane patches and imposed a pulling force to deform them into a tube, which might
269 undergo fission (Baoukina et al., 2012; Pinot et al., 2014) (**Figure 6A and B**). This approach is informative in
270 terms of membrane mechanics, but the 1:4 scale of the MARTINI force field (one elementary beads for 3 to
271 4 bonded atoms) makes the depiction of the chemistry of polyunsaturated phospholipids quite imprecise.
272 Nevertheless, we could construct PC bilayers in which acyl chains made of 4 or 5 beads approximate the
273 series 18:0-18:1, 18:0-18:2, 18:0-20:4 and 18:0-22:6 (**Figure 6A and B**). In the all-atom mode, we considered

membrane patches of 2 x 144 phospholipids with the same composition as that used in the experiments. This approach is limited to flat membranes but enables an accurate description of the slight chemical differences between polyunsaturated acyl chains (**Figure 6C-E**).

For all coarse-grained membranes tested, applying a constant force above a threshold of 175 kJ $mol^{-1}$ $nm^{-1}$ induced the formation of a tube, which grew by a fast protrusion phase followed by a linear phase as previously observed (Baoukina et al., 2012). Increasing the degree of phospholipid polyunsaturation (18:0-18:1 < 18:0-18:2 < 18:0-20:4 < 18:0-22:6) accelerated the linear phase and resulted in the formation of longer and thinner tubes (**Figure 6A and Figure 6-figure supplement 1A and B**). Because the bending energy of a membrane tube is proportional to the ratio between tube length and radius ($E_b = \pi K_b L/R$), we plotted $L/R$ as a function of the applied force (Figure 6A). At t = 200 ns and for $F$ = 200 KJ $mol^{-1}$ $nm^{-1}$, $L/R$ = 6, 12, 16 and 20 nm/nm for 18:0-18:1, 18:0-18:2, 18:0-20:4 and 18:0-22:6 tubes, respectively. Considering that these tubes should have stored the same curvature energy, these changes in L/R suggested inverse changes in membrane bending rigidity: 18:0-18:2, 18:0-20:4 and 18:0-22:6 membranes had relative values of $K_b$ equal to 50% 35% and 30% of $K_b$ for 18:0-18:1 membranes, respectively.

During the time of the simulations (200 ns), we observed fission events for some tubes formed from 18:0-20:4 and 18:0-22:6 membranes but not from 18:0-18:1 or 18:0-18:2 membranes (**Figure 6B, Figure 6-figure supplement 1A and Video 1**). Although the number of simulations did not allow us to establish robust statistics, we noticed that the force threshold at which fission occurred was lower for 18:0-22:6 membranes than for 18:0-20:4 membranes (**Figure 6B and Figure 6-figure supplement 1B**). Moreover, fission occurred sooner for 18:0-22:6 tubes as compared to 18:0-20:4 tubes. Thus, the coarse-grained simulations agreed well with the experiments: the propensity of membranes to undergo deformation and fission correlates with the unsaturation level of the phospholipid *sn2* acyl chain.

For all-atom bilayers, we focused on parameters informative for the tendency of the phospholipid acyl chains to depart from the straight conformation. This tendency allows phospholipids to adopt different shapes and, consequently, to reduce the stress induced by membrane curvature (Pinot et al., 2014). We determined (i) the speed at which the terminal $CH_3$ group moves along the membrane normal (*z* velocity) *vs* membrane plane (*x* velocity); (ii) the frequency of FA torsions (when the acyl chain displays an angle < 100°), (iii) the number of protrusions of the terminal $CH_3$ group above the glycerol during 100 ns; and (iv) the density of lipid packing defects, i.e. interfacial regions where aliphatic carbons are directly accessible to the solvent. **Figure 6C-E and Figure 6-figure supplement 2** show that whatever the parameter considered, the calculated value always increased with the polyunsaturation level of the *sn2* chain, with 22:6 clearly surpassing all other polyunsaturated FAs. In contrast, the behavior of the *sn1* 18:0 chain was relatively constant and appeared poorly dependent on the nature of the neighboring *sn2* chain. Altogether, these

various analyses show that the main effect of having an *sn2* polyunsaturated chain in phospholipids is to increase the probability of fast movements of along the *z*-axis.

To determine whether the membrane features endowed by the polyunsaturated acyl chain depend on its esterification at position *sn2* as observed in natural lipids, we performed molecular dynamics simulations on phospholipid bilayers in which we swapped the *sn1* and *sn2* acyl chains (**Figure 6-figure supplement 3**). In all atom simulations, we observed that the rough features distinguishing the saturated and the polyunsaturated acyl chains remained after having permutated their position. These include *z* velocity, acyl chain torsions, and number of protrusions (**Figure 6-figure supplement 3A)**. However, measurements of the acyl chain density across the bilayer indicated that acyl chain swapping modified the mean position of the saturated and polyunsaturated acyl chains across the bilayer (**Figure 6-figure supplement 3B)**. This effect probably resulted from the tilted orientation of glycerol, which makes the *sn1* and *sn2* positions not equivalent in term of *z* coordinates. In natural phospholipids, the density profile of the *sn1* saturated FA showed a peak in the bilayer center whereas the *sn2* polyunsaturated FA showed a characteristic dip. This shift indicates that the *sn1* saturated FA tail invaded the central region of the bilayer left vacant by the *sn2* polyunsaturated FA, which goes up (Eldho et al., 2003). With swapped 22:6-18:0 phospholipids, this difference in density disappeared and the membrane appeared thinner than with natural 18:0-22:6 phospholipids (**Figure 6-figure supplement 3B**). Thus, the relative esterification position of the saturated and polyunsaturated FAs in natural lipids facilitates compensatory *z* movements where the polyunsaturated FA explores the interfacial region while the saturated FA explores the bilayer center. In coarse-grained simulations, the propensity of the membrane to undergo tubulation and fission increased with the level of phospholipid polyunsaturation (18:1-18:0 < 20:4-18:0 < 22:6-18:0), i.e. the same trend as that observed on classical *sn1*-saturated-*sn2*-unsaturated membranes (**Figure 6-figure supplement 3C**). However, acyl chain swapping facilitated membrane fission (e.g. 22:6-18:0 > 18:0-22:6) (**Figure 6-figure supplement 3C** and **Video 2**). This difference might arise from the lack of compensatory *z* movements between the two acyl chains in swapped lipids that could render the bilayer more fragile and therefore more prone to undergo fission.

333 **Discussion**

334 Although a wealth of information is available on the interactions between endocytic proteins and specific
335 lipids (Puchkov and Haucke, 2013), the role of the hydrophobic membrane matrix has been poorly
336 investigated. In vivo, manipulating the acyltransferases that are responsible for the large differences in the
337 acyl chain profile of differentiated cells is challenging and is just starting to emerge (Hashidate-Yoshida et
338 al., 2015; Rong et al., 2015). *In vitro*, purified lipids are generally available from disparate sources (e.g. egg
339 PC, brain PS), implying different acyl chain profiles. Synthetic lipids provide the best alternative but the
340 most affordable ones generally display symmetric acyl chain combinations. This is exemplified by DOPS
341 (18:1-18:1 PS), which has allowed spectacular advances in our understanding of the structure of the
342 dynamin spiral (Chappie et al., 2011), but is very rare in mammalian membranes (Yabuuchi and O'Brien,
343 1968). Overall, the membrane templates on which dynamin and its partners have been studied are
344 generally ill defined in terms of acyl chain profiles. Our comprehensive analysis indicates that acyl chain
345 asymmetry and acyl chain polyunsaturation have major effects on the mechanical activity of dynamin.

346 A few studies have established that polyunsaturated phospholipids considerably modify the properties of
347 membranes (Armstrong et al., 2003; Eldho et al., 2003; Garcia-Manyes et al., 2010; Huang, 2001; Olbrich et
348 al., 2000; Rawicz et al., 2000). For LUVs, a high dithionite permeability of membranes containing 18:3-18:3
349 phospholipids has been reported (Armstrong et al., 2003). For GUVs, micropipette manipulations indicate
350 that the presence of at least one polyunsaturated acyl chain results in a drop of the membrane bending
351 modulus whereas the presence of two polyunsaturated acyl chains causes a jump in water permeability
352 (Olbrich et al., 2000; Rawicz et al., 2000). These pioneer studies were performed on membranes made of a
353 single lipid (PC) with a limited combination of acyl chains and in the absence of mechanically active proteins.
354 By using lipid mixtures covering a larger spectrum of acyl chain profiles and by including membrane
355 shaping/fission proteins, our study underlines the importance of both phospholipid polyunsaturation and
356 phospholipid acyl chain asymmetry in membrane mechanics.

357 Depending on its acyl chain profile, a membrane can be either very resistant or very permissive to dynamin-
358 mediated membrane vesiculation despite harboring the proper repertoire of polar head groups for protein
359 recruitment. However, these manipulations can also cause large changes in membrane permeability. Our
360 analysis uncovers a narrow chemical window that allows phospholipid membranes to be both highly
361 deformable and still impermeable to small solutes. Membranes with asymmetric saturated-polyunsaturated
362 phospholipids such as 18:0-20:4 or 18:0-22:6 phospholipids are much less leaky than membranes with
363 symmetrical 20:4-20:4 or 22:6-22:6 phospholipids but can still be readily vesiculated by dynamin provided
364 that BAR-domain proteins are present. Evidently, these features are advantageous for membranes such as
365 synaptic membranes that undergo super-fast endocytosis (Boucrot and Watanabe, 2017). Furthermore, the
366 fact that membranes with 18:0-22:6 phospholipids are systematically more permissive to the mechanical

367 activity of dynamin and endophilin than membranes with 18:0-20:4 phospholipids is of interest given the
368 importance of the omega-6/omega-3 ratio for health and notably for brain function.

369 The distinctive chemical feature of polyunsaturated acyl chains is the presence of saturated carbons ($CH_2$)
370 sandwiched between two unsaturated ones (=CH-$CH_2$-CH=). Rotational freedom around these $CH_2$ groups is
371 exceptionally high as compared to rotation around the $CH_2$ groups of monounsaturated or saturated acyl
372 chains (Feller et al., 2002). Our MD simulations indicate that motions of the acyl chain along the normal of
373 the membrane (*z* movements) increase in speed and in amplitude with the level acyl chain polyunsaturation
374 (18:2 < 18:3 < 20:4 < 22:6). Such movements should allow phospholipids to readily adapt their conformation
375 to membrane curvature (Barelli and Antonny, 2016; Pinot et al., 2014), hence explaining the gradual
376 decrease in membrane bending rigidity. Concurrently, the presence of a neighboring saturated acyl chain
377 should secure lipid packing and prevents the passage of small molecules. Whether this model also accounts
378 for the facilitation of the fission step per se remains, however, difficult to assess. This step involves a change
379 in membrane topology for which rare events such as protrusions of the terminal $CH_3$ groups could be
380 decisive as they could nucleate bilayer merging or favor friction effects by proteins (Simunovic et al., 2017).

381 Other variations in the acyl chain content of mammalian phospholipids will deserve further investigations.
382 First, we did not consider C22:5 acyl chains (omega-6 or omega-3), which are closer to C22:6 than C20:4
383 (Eldho et al., 2003). Although not abundant, C22:5 acyl chains are present in brain phospholipids (Yabuuchi
384 and O'Brien, 1968). Second, we did not study the influence of the linkage between the acyl chains and
385 glycerol. Plasmalogens, which form a large subclass of PE in the brain, harbor a *sn1* saturated acyl chain that
386 is bound to the glycerol through an ether-vinyl bond. Interestingly, ether-vinyl phospholipids considerably
387 decrease the permeability of model membranes to ions because these lipids pack more tightly than their
388 ester counterparts (Zeng et al, 1998). The influence of plasmalogens on membrane flexibility and fission
389 remains to be investigated. Last, we only partially addressed the bias observed in natural phospholipids,
390 where saturated and polyunsaturated acyl chains are preferentially esterified on different positions of the
391 glycerol backbone (*sn1* and *sn2*, respectively). Our simulations suggest that some general traits provided by
392 the combination of one saturated acyl chain and one unsaturated acyl chain are preserved when the acyl
393 chains are swapped between the *sn1* and *sn2* positions; notably the fact that membrane deformation and
394 fission is facilitated by the level of polyunsaturation (18:1-18:0 < 20:4-18:0 < 22:6-18:0). However, coarse-
395 grained simulations also suggest that artificial *sn1*-polyunsaturated-*sn2*-saturated phospholipids make
396 membranes more amenable to vesiculation than their natural *sn1*-saturated-*sn2*-polyunsaturated
397 counterparts. Testing this hypothesis by *in vitro* reconstitutions will require considerable efforts in lipid
398 synthesis since swapped phospholipids are not commercially available.

399 The abilities to vesiculate and to act as selective barriers are two fundamental properties of cellular
400 membranes. Without membrane vesiculation, a cell cannot divide; without selective permeability, it cannot

401 control the concentration of its nutrients. Experiments aimed at mimicking the emergence of primitive
402 membranes have illuminated how these properties need to be finally balanced. Single chain amphiphilic
403 molecules (e.g. fatty acids), the most plausible building blocks for primitive membranes, can self-assemble
404 into bilayers, which spontaneously vesiculate (Bruckner et al., 2009). However, these bilayers are very leaky
405 to even large solutes (in the $10^3$ Da range). Later, the shift from single chain to dual chain lipids has probably
406 allowed primitive cells to reduce the general permeability of their membrane, thereby imposing an
407 evolutionary pressure for the emergence of specialized transporters (Budin and Szostak, 2011). The
408 experiments presented here suggest that phospholipids with one saturated and one polyunsaturated acyl
409 chain, which are absent in many eukaryotes (e.g. yeast) but abundant in some highly differentiated cells
410 (e.g. neurons, photoreceptors, sperm) provide a solution to an early dilemma in evolution: finding the right
411 balance between efficient membrane vesiculation without loss in membrane permeability. Moreover, the
412 fact that saturated-DHA (omega-3) phospholipids are systematically better for membrane vesiculation than
413 many other saturated-polyunsaturated phospholipids, including saturated-arachidonate (omega-6), is
414 informative considering the importance of the omega-6/omega-3 ratio for health.

415

## MATERIAL and METHODS

***Key Resources Table***

| Reagent type (species) or resource | Designation | Source or reference | Identifiers | Additional information |
|---|---|---|---|---|
| Phosphatidylcholine | 1-stearoyl-2-oleoyl-sn-glycero-3-phosphocholine | Avanti Polar Lipids | Ref 18:0-18:1 PC \| 850467 | |
| Phosphatidylcholine | 1-stearoyl-2-linoleoyl-sn-glycero-3-phosphocholine | Avanti Polar Lipids | Ref 18:0-18:2 PC \| 850468 | |
| Phosphatidylcholine | 1-stearoyl-2-linolenoyl-sn-glycero-3-phosphocholine | Avanti Polar Lipids | | 18:0-18:3 PC Custom |
| Phosphatidylcholine | 1-stearoyl-2-arachidonoyl-sn-glycero-3-phosphocholine | Avanti Polar Lipids | Ref 18:0-20:4 PC \| 850469 | |
| Phosphatidylcholine | 1-stearoyl-2-docosahexaenoyl-sn-glycero-3-phosphocholine | Avanti Polar Lipids | Ref 18:0-22:6 PC \| 850472 | |
| Phosphatidylcholine | 1,2-dimyristoyl-sn-glycero-3-phosphocholine | Avanti Polar Lipids | Ref 14:0 PC (DMPC) \| 850345 | |
| Phosphatidylcholine | 1,2-dioleoyl-sn-glycero-3-phosphocholine | Avanti Polar Lipids | Ref 18:1 (Δ9-Cis) PC (DOPC) \| 850375 | |
| Phosphatidylcholine | 1,2-dilinoleoyl-sn-glycero-3-phosphocholine | Avanti Polar Lipids | Ref 18:2 (Cis) PC (DLPC) \| 850385 | |
| Phosphatidylcholine | 1,2-diarachidonoyl-sn-glycero-3-phosphocholine | Avanti Polar Lipids | 20:4 (Cis) PC \| 850397 | |
| Phosphatidylcholine | 1,2-didocosahexaenoyl-sn-glycero-3-phosphocholine | Avanti Polar Lipids | 22:6 (Cis) PC \| 850400 | |
| Phosphoethanolamine | 1-stearoyl-2-oleoyl-sn-glycero-3-phosphoethanolamine | Avanti Polar Lipids | 18:0-18:1 PE \| 850758 | |
| Phosphoethanolamine | 1-stearoyl-2-linoleoyl-sn-glycero-3-phosphoethanolamine | Avanti Polar Lipids | 18:0-18:2 PE \| 850802 | |
| Phosphoethanolamine | 1-stearoyl-2-linolenoyl-sn-glycero-3-phosphoethanolamine | Avanti Polar Lipids | | 18:0-18:3 PE Custom |
| Phosphoethanolamine | 1-stearoyl-2-arachidonoyl-sn-glycero-3-phosphoethanolamine | Avanti Polar Lipids | Ref 18:0-20:4 PE \| 850804 | |
| Phosphoethanolamine | 1-stearoyl-2-docosahexaenoyl-sn-glycero-3-phosphoethanolamine | Avanti Polar Lipids | Ref 18:0-22:6 PE \| 850806 | |
| Phosphoethanolamine | 1,2-dimyristoyl-sn-glycero-3-phosphoethanolamine | Avanti Polar Lipids | Ref 14:0 PE \| 850745 | |
| Phosphoethanolamine | 1,2-dioleoyl-sn-glycero-3-phosphoethanolamine | Avanti Polar Lipids | Ref 18:1 (Δ9-Cis) PE (DOPE) \| 850725 | |
| Phosphoethanolamine | 1,2-dilinoleoyl-sn-glycero-3-phosphoethanolamine | Avanti Polar Lipids | Ref 18:2 PE \| 850755 | |
| Phosphoethanolamine | 1,2-diarachidonoyl-sn-glycero-3-phosphoethanolamine | Avanti Polar Lipids | Ref 20:4 PE \| 850800 | |
| Phosphoethanolamine | 1,2-didocosahexaenoyl-sn-glycero-3-phosphoethanolamine | Avanti Polar Lipids | Ref 22:6 PE \| 850797 | |
| Phosphatidylserine | 1-stearoyl-2-oleoyl-sn-glycero-3-phospho-L-serine | Avanti Polar Lipids | Ref 18:0-18:1 PS \| 840039 | |
| Phosphatidylserine | 1-stearoyl-2-linoleoyl-sn-glycero-3-phospho-L-serine | Avanti Polar Lipids | Ref 18:0-18:2 PS \| 840063 | |
| Phosphatidylserine | 1-stearoyl-2-linolenoyl-sn-glycero-3-phospho-L-serine | Avanti Polar Lipids | | 18:0-18:3 PS Custom |
| Phosphatidylserine | 1-stearoyl-2-arachidonoyl-sn-glycero-3-phospho-L-serine | Avanti Polar Lipids | Ref 18:0-20:4 PS \| 840064 | |
| Phosphatidylserine | 1-stearoyl-2-docosahexaenoyl-sn-glycero-3-phospho-L-serine | Avanti Polar Lipids | Ref 18:0-22:6 PS \| 840065 | |
| Phosphatidylserine | 1,2-dimyristoyl-sn-glycero-3-phospho-L-serine | Avanti Polar Lipids | Ref 14:0 PS \| 840033 | |
| Phosphatidylserine | 1,2-dioleoyl-sn-glycero-3-phospho-L-serine | Avanti Polar Lipids | Ref 18:1 PS (DOPS) \| 840035 | |
| Phosphatidylserine | 1,2-dilinoleoyl-sn-glycero-3-phospho-L-serine | Avanti Polar Lipids | Ref 18:2 PS \| 840040 | |
| Phosphatidylserine | 1,2-diarachidonoyl-sn-glycero-3-phospho-L-serine | Avanti Polar Lipids | Ref 20:4 PS \| 840066 | |
| Phosphatidylserine | 1,2-didocosahexaenoyl-sn-glycero-3-phospho-L-serine | Avanti Polar Lipids | Ref 22:6 PS \| 840067 | |

### ***Protein purification and labelling***

419 Proteins were purified as described (Pinot et al., 2014; Stowell et al., 1999). Dynamin was purified from rat
420 brain using a recombinant amphiphysin-2 SH3 domain as an affinity ligand. Brain extracts were incubated
421 with 10 mg ml-1 glutathione-S-transferase-tagged amphiphysin-2 SH3 domain on glutathione–agarose
422 beads at 4°C. After extensive washing of the matrix in buffer A (100 mM NaCl, 20 mM HEPES, pH 7.3, 1 mM
423 dithiothreitol (DTT)), dynamin was eluted in 3 ml buffer B (1.2 M NaCl, 20 mM HEPES, pH 6.5, 1mM DTT),
424 and dialysed overnight into 200 mM NaCl, 20 mM HEPES, 20% glycerol. Full-length mouse endophilin A1 in
425 pGEX-6p1 (gift of A. Schmidt) was expressed in E coli for 3 h at 37°C after induction with 1 mM IPTG. Cells
426 were lysed in 50 mM Tris pH 7.4, 150 mM NaCl using a French press in the presence of antiproteases and
427 spun at 40,000 rpm for 30 min at 4°C. The supernatant was incubated with glutathione-Sepharose 4B beads
428 followed by extensive washes in lysis buffer. PreScission protease was directly added to the beads at 4°C
429 overnight under gentle agitation to cleave the fusion protein. Endophilin was recovered in supernatant and
430 further purified on a Superdex 200 column in 20 mM Tris pH 7.4, 300 mM KCl, 5 mM imidazole, 1 mM DTT.

431 ***Preparation of liposomes***

432 Lipids were purchased from Avanti Polar Lipids as chloroform solutions (see Key resources table). These
433 included the following species of phosphatidylcholine (PC), phosphatidylethanolamine (PE) and
434 phosphatidylserine (PS): 14:0-14:0, 18:0-18:1, 18:1-18:1, 18:0-18:2, 18:2-18:2, 18:0-18:3, 18:0-20:4, 20:4-
435 20:4, 18:0-22:6 and 22:6-22:6. Note that 18:0-18:3 phospholipid species were custom-made lipids from
436 Avanti. Phosphatidylinositol (4,5)bisphosphate ($PIP_2$) was from natural source (brain). Submicrometer
437 liposomes used for biochemical experiments and for electron microscopy were prepared by extrusion. A
438 lipid film containing phospholipids and cholesterol at the desired molar ratio (**see Table S1-3 in**
439 **supplementary file 1**) was formed in a rotary evaporator and hydrated at a final lipid concentration of 1
440 mM in a freshly degassed HK buffer (50 mM Hepes pH 7.2, 120 mM K Acetate) supplemented with 1 mM
441 DTT. The suspension was submitted to five cycles of freezing and thawing and stored at -20 °C under argon
442 to avoid lipid oxidation. Calibrated liposomes were obtained by extrusion through 400 or 100 nm
443 polycarbonate filters using a hand extruder (Avanti Polar Lipids). The size distribution of the liposomes was
444 determined by dynamic light scattering at a final concentration of 0.1 mM lipids in HK buffer. All liposome
445 suspensions were used within 1-2 days after extrusion. Special care was taken to minimize lipid oxidation by
446 using fleshly degassed buffer (supplemented with 1 mM DTT) and by storing the liposome suspensions
447 under argon.

448 ***Preparation of GUVs***

449 Giant unilamellar vesicles were generated by electroformation as described (Pinot et al., 2014) with the
450 following modifications. Lipid mixtures (0.5 mg/ml; **see Table S4 in supplementary file 1**) in chloroform
451 were deposited on indium tin oxide coated glass slides at 50°C to prevent lipid de-mixing and dried under

452 vacuum for 1h to remove all solvents. After this step sucrose 250 mM osmotically equilibrated with buffers
453 was added to the chamber. GUVs were electroformed (Angelova et al., 1992) with Vesicle Prep Pro (Nanion
454 Technologies GmbH, Munich, Germany), applying an AC electric field with 3 V and 5 Hz for 218 min at 37°C.

455 ***GTPase assay***

456 GTP hydrolysis in dynamin was measured using a colorimetric assay (Leonard et al., 2005). The sample (60
457 µl) initially contained 400 nm extruded liposomes (0.1 mM) of defined composition (see Table S1-3) in HK
458 buffer supplemented with 2.5 mM $MgCl_2$, 1 mM DTT and 500 µM GTP. Just before measurement,
459 endophilin (0.6 µM) was added and the reaction was initiated by the addition and mixing of 0.3 µM
460 dynamin. At the indicated times (15, 45, 75, 120, 180, 240 and 360 seconds), aliquots (7.5 µl) were
461 withdrawn and immediately mixed with a drop of EDTA (5 µl, 250 mM) in a 96 well plate. At the end of the
462 experiment, 150 µl of a malachite green stock solution was added to each well and the absorbance at 650
463 nm was measured using a microplate reader and compared to that of a standard curve of phosphate (0 –
464 200 µM) in order to determine the concentration of GTP hydrolyzed by dynamin.

465 ***Push-pull pyrene (PA) fluorescence on LUVs***

466 Fluorescence spectra of the PA probe with liposomes was performed as described (Niko et al., 2016). The
467 sample (600 µl) initially contained 0.1 mM extruded liposomes (100 nm) of defined composition (see Table
468 S1). After 5 min incubation of the liposomes solution with 1 µM PA probe at 37 °C, a fluorescence emission
469 spectrum (450 – 700 nm; bandwidth 1 nm) was recorded upon excitation at 430 nm (bandwidth 5 nm). All
470 spectra were corrected for the corresponding blank (suspension of liposomes without the probe).

471 ***Dithionite-mediated NBD quenching assay***

472 The extent of dithionite quenching of the NBD-labeled PE was performed as described (Angeletti and
473 Nichols, 1998). Briefly, the sample (600 µl) that initially contained 400 nm extruded liposomes (0.1 mM) of
474 defined composition (see Table S2) were let equilibrating in HK buffer 5 min at 37°C with 600 rpm stirring.
475 After 30 sec of fluorescence measurements (excitation 505 nm, bandwidth 1 nm; emission 540 nm,
476 bandwidth 10 nm) NBD quenching was started by adding 10 mM dithionite and the reaction was followed
477 during 5 min at 37°C with 600 rpm stirring. The percentage of NBD quenching was calculated by the
478 equation: Quenching NBD (%) = $(F_i – F_0) / (F_T – F_0) \times 100$ where $F_0$ corresponds to the fluorescence of the
479 vesicles at time 0-30 sec; $F_i$ is the fluorescence after a certain period of incubation with dithionite, and $F_T$ is
480 the maximum quenching that corresponds to the fluorescence value obtained after addition of 0.1% Triton
481 X-100.

482 ***Electron microscopy***

483 Mixtures containing liposomes, dynamin, endophilin and nucleotides were prepared in HK buffer
484 supplemented with 2.5 mM MgCl2 and 1 mM DTT (final volume 50 µl). For the tubulation experiments in
485 presence of the non-hydrolyzable analog GTPγS, vesicles were incubated for 5 or 15 min at room
486 temperature. For the fission experiments in presence of GTP, vesicles were incubated for 30 min at room
487 temperature. Thereafter, an EM grid was put on the protein-liposome mixture for 5 min, rinsed with a
488 droplet of 100 mM Hepes (pH 7.0) for 1 min, and then stained with 1% uranyl acetate. The grid was
489 observed in a JEOL JEM1400 transmission electron microscope equipped with a MORADA SIS camera. To
490 determine the size distribution of the liposomes or of the protein-liposome profiles, 500 to 1000 profiles for
491 each condition and from three independent experiments were analyzed using the ellipse tool of the NIH
492 Image J software. The apparent radius was calculated as R=(A/π)1/2 where A is the apparent area of the
493 profile. All experiments were performed with 0.5 µM dynamin, 1 µM endophilin, 500 µM nucleotide and 0.1
494 mM lipids.

495 ***GUV permeability and size assay***

496 GUV permeability was studied in 18:0-22:6 and 22:6-22:6 liposomes using a previously developed assay
497 with some modifications (Jiménez-Rojo et al., 2014). After GUVs stabilization soluble Alexa488 was
498 externally added to follow the entrance of the probe over time. After 15 min incubation, vesicles were
499 imaged by confocal microscopy and permeability was quantified using the following equation: Permeability
500 (%) = Iin/Iex x 100 where Iin is the average of the fluorescence inside the individual GUV and Iex is the
501 average of external fluorescence of the probe in solution.

502 Membrane fission induced by dynamin and endophilin in the presence of GTP was followed indirectly by
503 monitoring the size of GUVs over time since the vesicles produced by the proteins are too small to be
504 optically resolved. We used a previously developed assay with some modifications (Meinecke et al., 2013).
505 After GUVs stabilization, dynamin, endophilin and GTP were added and incubated for 1 hour at 37°C before
506 and imaging by confocal microscopy. All experiments were performed with 0.5 µM dynamin, 1 µM
507 endophilin, 500 µM nucleotide and 0.1 mM lipids. Shrinking percentage was calculated by the equation:
508 Shrinking (%) = 100 x A0/Ai where A0 is the vesicles area at time 0 and Ai is vesicles area after a defined
509 period of incubation.

510 ***Molecular dynamics***

511 All-atom simulations were performed with GROMACS 5 (Abraham et al., 2015) software and CHARMM36
512 (Klauda et al., 2010) force field. The various systems were built with the Charmm-Gui tool (Lee et al., 2015)
513 with 33% Cholesterol, 1% PI(4,5)$P_2$, and with 30% PS, 20% PE, and 16% PC, harboring defined acyl chains
514 (18:0-18:1, 18:0-18:2, 18:0-18:3, 18:0-20:4, 18:0-22:6, 14:0-14:0, 18:2-18:2, 20:4-20:4, 22:6-22:6). Lipids not
515 present in the Charmm-Gui database (18:0-18:2, 18:0-18:3, 18:2-18-2 and 22:6-22:6 and swapped lipids)

516 were built by adding unsaturations to related lipids (i.e. 18:0-18:1, 18:1-18:1 or 22:1-22:1). Note that one of
517 this lipid (18:0-18:2) is now present in the database and has the same topology as the one used here. The
518 bilayers contained 2 x 144 phospholipids with counter ions to neutralize the system and with 120 mM NaCl.

519 The simulation parameters were those of Charmm-Gui under semi isotropic conditions within the NPT
520 ensemble: *x* and *y* directions were coupled, whereas *z* direction was independent. Periodic boundaries
521 applied to all directions. We first equilibrated the membranes for 200 ps using the standard Charmm-Gui
522 six-step process during which constraints on lipids were gradually released. Next, an additional equilibration
523 step was performed to equilibrate the TIP3P model of water. All simulations were equilibrated using the
524 Berendsen thermostat and barostat at 303 K and 1 bar, respectively, except for 14:0-14:0 bilayers, which
525 were equilibrated at 310 K. Lipids and water + ions were coupled separately.

526 Production runs were performed with the V-rescale thermostat at 303 K except for 14:0-14:0 bilayers (310
527 K). The Parrinello-Rahman thermostat was used to stabilize the pressure at 1 bar with a time constant of 5
528 ps and a compressibility of 4.5 x $10^{-5}$ $bar^{-1}$ (Parrinello and Rahman, 1981). Again, lipids and water + ions
529 were coupled separately. The time step was set at 2 fs. Bond lengths were constrained using the P-LINCS
530 algorithm (Hess, 2008). Cutoff was fixed at 1.2 nm for the Lennard-Jones and electrostatic interactions. The
531 smooth particle-mesh was used to evaluate the electrostatic interactions. Frames were saved every 10 ps.

532 Trajectory analyses were performed from 400 ns simulations from which we discarded the first 100 ns in
533 order to rule out processes that are not at equilibrium. The remaining 300 ns trajectory was divided in 3
534 blocks of 100 ns to determine the standard deviation. Frames were analyzed every 100 ps except for the
535 velocity and permeability analysis for which we used 10 ps frames.

536 Coarse-grained simulations were performed with GROMACS 4.5 (Hess et al., 2008) using the Martini force
537 field (Wassenaar et al., 2015). The systems were built with the Charmm-Gui tool adapted to coarse-grained
538 simulations (Qi et al., 2015). In all simulations, we varied the acyl chains composition while keeping the PC
539 polar head constant. We used four lipids to approximate the asymmetric lipids 18:0-18:1, 18:0-18:2, 18:0-
540 20:4, and 18:0-22:6. Note that the coarse-grained simplification does not distinguish C16:0 from C18:0,
541 C20:4 from C22:5, and C22:6 from C20:5. We built coarse-grained models of swapped phospholipids from
542 natural phospholipids having acyl chains of the same length. The systems contained 18 000 lipids and were
543 solvated with a 100 nm thick layer of water.

544 The sytems were equilibrated with the standard Charmm-Gui six-step process. Production runs were
545 performed with the V-rescale thermostat at 303K. The Berendsen barostat was used to stabilize the
546 pressure at 1bar with a time constant of 4ps and compressibility of 5 x 10-5 $bar^{-1}$ (Berendsen et al., 1984).
547 The different membranes were simulated under a semi-isotropic condition and the periodic boundaries
548 were applied in all directions. Lipids and water/ions were coupled separately. The time step was fixed at 20

549 fs and the cutoff for the Lennard-Jones and electrostatic interactions was set at 1.2nm. The smooth particle-
550 mesh was used to evaluate the electrostatic interactions.

551 To simulate membrane deformation and fission, we applied a force perpendicular to the initially flat bilayer
552 (Baoukina et al, 2012). The force (from 175 to 250 KJ $mol^{-1}$ $nm^{-1}$) was applied to the center of mass of a lipid
553 patch of radius = 3 nm, in which lipids were restrained in the lateral (*x,y*) directions. The simulations were
554 performed for 200 ns and were repeated two to three times under most conditions.

555 For further information on all molecular dynamics simulations, refer to the Gromacs mdp files
556 (**supplementary files 2 and 3**).

557 **Simulation analysis**

558 To evaluate membrane permeability, we counted the number of water molecule(s) that have visited the
559 center of membrane (corresponding to 65% of the thickness) during 100 ns time frames. These water
560 molecules were separated in two classes: those that fully crossed the bilayer and those that entered the
561 hydrophobic region and then exited from the same side. Results were normalized to the total number of
562 water molecules. The velocity rate of the terminal methyl group of the acyl chains was calculated from the
563 sum of distances traveled by each methyl group in the x or in the *z* direction every 10 ps. For protrusions,
564 we calculated the number of events during 100 ns blocks where the CH3 terminal group of the acyl chain
565 reached a *z* position above the central carbon of glycerol from the same lipid. An acyl chain torsion
566 corresponds to an angle below 100° between carbons that have relative positions of n-2, n and n+2 along
567 the acyl chain. Packing defect analysis was performed as previously described (Vamparys et al., 2013). This
568 membrane scanning procedure allows the detection of aliphatic atoms that are directly accessible to the
569 solvent and that are either < 1Å (shallow defect) or > 1Å (deep defect) below the nearest glycerol.

570

**ACKNOWLEDGEMENTS**

We thank Andrey Klymchenko for the PA probe, Wen-Ting Lo and Volker Haucke for the SNX9 protein, Guillaume Drin for help with GUVs preparation and Alenka Copic for comments on the manuscript. We are very grateful to Hugues Chap, Michel Lagarde, and Gérard Lambeau for their insights into the history of acyl chain asymmetry of phospholipids. This work was supported in part by an ERC grant (268 888) and is currently supported by the Agence Nationale de la Recherche (ANR-11-LABX-0028-01) and the HPC resources of CINES under the allocations 2016-c2016077362 and 2017-A0020707362 made by GENCI. M.M. is supported by a postdoctoral fellowship from the Basque Government.

579 **REFERENCES**


580 Abraham, M., Hess, B., Spoel, D., and Lindahl, E. (2015). GROMACS User Manual version 5.0. 1. 2014.

581 Angeletti, C., and Nichols, J. W. (1998). Dithionite quenching rate measurement of the inside-outside
582 membrane bilayer distribution of 7-nitrobenz-2-oxa-1, 3-diazol-4-yl-labeled phospholipids. Biochemistry
583 37:15114-19.

584 Angelova, M., Soléau, S., Méléard, P., Faucon, F., and Bothorel, P. (1992). Preparation of giant vesicles by
585 external AC electric fields. Kinetics and applications. In Trends in Colloid and Interface Science VI (pp. 127-
586 131): Springer.

587 Antonny, B., Burd, C., De Camilli, P., Chen, E., Daumke, O., Faelber, K., et al. (2016). Membrane fission by
588 dynamin: what we know and what we need to know. EMBO J 35:2270-84.

589 Armstrong, V. T., Brzustowicz, M. R., Wassall, S. R., Jenski, L. J., and Stillwell, W. (2003). Rapid flip-flop in
590 polyunsaturated (docosahexaenoate) phospholipid membranes. Arch Biochem Biophys 414:74-82.

591 Baoukina, S., Marrink, S. J., and Tieleman, D. P. (2012). Molecular structure of membrane tethers. Biophys J
592 102:1866-71. doi: 10.1016/j.bpj.2012.03.048.

593 Barelli, H., and Antonny, B. (2016). Lipid unsaturation and organelle dynamics. Curr Opin Cell Biol 41:25-32.
594 doi: 10.1016/j.ceb.2016.03.012.

595 Bazinet, R. P., and Layé, S. (2014). Polyunsaturated fatty acids and their metabolites in brain function and
596 disease. Nat Rev Neurosci 15:771-85. doi: 10.1038/nrn3820.

597 Berendsen, H. J. C., Postma, J. P. M., van Gunsteren, W. F., DiNola, A., and Haak, J. R. (1984). Molecular
598 dynamics with coupling to an external bath. J Chem Phys 81:3684-90. doi: 10.1063/1.448118.

599 Boesze-Battaglia, K., and Schimmel, R. (1997). Cell membrane lipid composition and distribution:
600 implications for cell function and lessons learned from photoreceptors and platelets. J Exp Biol 200:2927-36.

601 Boucrot, E., Ferreira, A. P., Almeida-Souza, L., Debard, S., Vallis, Y., Howard, G., et al. (2015). Endophilin
602 marks and controls a clathrin-independent endocytic pathway. Nature 517:460-5. doi:
603 10.1038/nature14067.

604 Boucrot, E., and Watanabe, S. (2017). Fast and ultrafast endocytosis. Curr Opin Cell Biol 47:64-71. doi:
605 10.1016/j.ceb.2017.02.013.

606 Bruckner, R., Mansy, S., Ricardo, A., Mahadevan, L., and Szostak, J. (2009). Flip-flop-induced relaxation of
607 bending energy: implications for membrane remodeling. Biophys J 97:3113-22. doi:
608 10.1016/j.bpj.2009.09.025.

609 Budin, I., and Szostak, J. W. (2011). Physical effects underlying the transition from primitive to modern cell
610 membranes. Proc Natl Acad Sci USA 108:5249-54. doi: 10.1073/pnas.1100498108.

611 Chappie, J. S., Mears, J. A., Fang, S., Leonard, M., Schmid, S. L., Milligan, R. A., et al. (2011). A pseudoatomic
612 model of the dynamin polymer identifies a hydrolysis-dependent powerstroke. Cell 147:209-22. doi:
613 10.1016/j.cell.2011.09.003.

614 Danino, D., Moon, K.-H., and Hinshaw, J. E. (2004). Rapid constriction of lipid bilayers by the
615 mechanochemical enzyme dynamin. J Struct Biol 147:259-67.

616 Eldho, N. V., Feller, S. E., Tristram-Nagle, S., Polozov, I. V., and Gawrisch, K. (2003). Polyunsaturated
617 docosahexaenoic *vs* docosapentaenoic acid differences in lipid matrix properties from the loss of one
618 double bond. J Am Chem Soc 125:6409-21.

619 Farsad, K., Ringstad, N., Takei, K., Floyd, S. R., Rose, K., and De Camilli, P. (2001). Generation of high
620 curvature membranes mediated by direct endophilin bilayer interactions. J Cell Biol 155:193-200.

621 Feller, S. E., Gawrisch, K., and MacKerell, A. D. (2002). Polyunsaturated fatty acids in lipid bilayers: intrinsic
622 and environmental contributions to their unique physical properties. J Am Chem Soc 124:318-26.

623 Garcia-Manyes, S., Redondo-Morata, L., Oncins, G., and Sanz, F. (2010). Nanomechanics of lipid bilayers:
624 heads or tails? J Am Chem Soc 132:12874-86. doi: 10.1021/ja1002185.

625 Hanahan, D. J., Brockerhoff, H., and Barron, E. J. (1960). The site of attack of phospholipase (lecithinase) A
626 on lecithin: a re-evaluation Position of fatty acids on lecithins and triglycerides. J Biol Chem 235:1917-23.

627 Harayama, T., Eto, M., Shindou, H., Kita, Y., Otsubo, E., Hishikawa, D., et al. (2014). Lysophospholipid
628 acyltransferases mediate phosphatidylcholine diversification to achieve the physical properties required in
629 vivo. Cell Metab 20:295-305. doi: 10.1016/j.cmet.2014.05.019.

630 Hashidate-Yoshida, T., Harayama, T., Hishikawa, D., Morimoto, R., Hamano, F., Tokuoka, S. M., et al. (2015).
631 Fatty acyl-chain remodeling by LPCAT3 enriches arachidonate in phospholipid membranes and regulates
632 triglyceride transport. Elife 4. doi: 10.7554/eLife.06328.

633 Hess, B., Kutzner, C., Van Der Spoel, D., and Lindahl, E. (2008). GROMACS 4: algorithms for highly efficient,
634 load-balanced, and scalable molecular simulation. J Chem Theory Comput 4:435-47. doi:
635 10.1021/ct700301q.

636 Hess, B. (2008). P-LINCS: A Parallel Linear Constraint Solver for Molecular Simulation. J Chem Theory
637 Comput 4:116-22. doi: 10.1021/ct700200b.

638 Huang, C.-h. (2001). Mixed-chain phospholipids: structures and chain-melting behavior. Lipids 36:1077-97.

639 Hulbert, A. (2003). Life, death and membrane bilayers. J Exp Biol 206:2303-11.

640 Jiménez-Rojo, N., Sot, J., Viguera, A. R., Collado, M. I., Torrecillas, A., Gómez-Fernández, J., et al. (2014).
641 Membrane permeabilization induced by sphingosine: effect of negatively charged lipids. Biophys J
642 106:2577-84. doi: 10.1016/j.bpj.2014.04.038.

643 Kamal, M. M., Mills, D., Grzybek, M., and Howard, J. (2009). Measurement of the membrane curvature
644 preference of phospholipids reveals only weak coupling between lipid shape and leaflet curvature. Proc Natl
645 Acad Sci USA 106:22245–50. doi: 10.1073/pnas.0907354106.

646 Klauda, J. B., Venable, R. M., Freites, J. A., O'Connor, J. W., Tobias, D. J., Mondragon-Ramirez, C., et al.
647 (2010). Update of the CHARMM all-atom additive force field for lipids: validation on six lipid types. J Phys
648 Chem B 114:7830-43. doi: 10.1021/jp101759q.

649 Lands, W. (1963). Reactivity of various acyl esters of coenzyme A with alpha'-acylglycerophosphorylcholine,
650 and positional specificities in lecithin synthesis. J Biol Chem 238:898-904.

651 Lee, J., Cheng, X., Swails, J. M., Yeom, M. S., Eastman, P. K., Lemkul, J. A., et al. (2015). CHARMM-GUI input
652 generator for NAMD, GROMACS, AMBER, OpenMM, and CHARMM/OpenMM simulations using the
653 CHARMM36 additive force field. J Chemical Theory Comput 12:405-13. doi: 10.1021/acs.jctc.5b00935.

654 Leonard, M., Song, B. D., Ramachandran, R., and Schmid, S. L. (2005). Robust colorimetric assays for
655 dynamin's basal and stimulated GTPase activities. Methods Enzymol 404:490-503.

656 Liu, Y.-W., Neumann, S., Ramachandran, R., Ferguson, S. M., Pucadyil, T. J., and Schmid, S. L. (2011).
657 Differential curvature sensing and generating activities of dynamin isoforms provide opportunities for
658 tissue-specific regulation. Proc Natl Acad Sci USA 108:E234–42. doi: 10.1073/pnas.

659 Manneville, J.-B., Casella, J.-F., Ambroggio, E., Gounon, P., Bertherat, J., Bassereau, P., Cartaud, J., Antonny
660 B., Goud, B. (2008). COPI coat assembly occurs on liquid-disordered domains and the associated membrane

661 deformations are limited by membrane tension. Proc Natl Acad Sci USA 105:16946-51.
662 doi:10.1073/pnas.0807102105.

663 Marszalek, J. R., and Lodish, H. F. (2005). Docosahexaenoic acid, fatty acid–interacting proteins, and
664 neuronal function: breastmilk and fish are good for you. Annu Rev Cell Dev Biol 21:633-57.

665 Meinecke, M., Boucrot, E., Camdere, G., Hon, W.-C., Mittal, R., and McMahon, H. T. (2013). Cooperative
666 recruitment of dynamin and BIN/amphiphysin/Rvs (BAR) domain-containing proteins leads to GTP-
667 dependent membrane scission. J Biol Chem 288:6651-61. doi: 10.1074/jbc.M112.444869.

668 Morlot, S., Galli, V., Klein, M., Chiaruttini, N., Manzi, J., Humbert, F., et al. (2012). Membrane shape at the
669 edge of the dynamin helix sets location and duration of the fission reaction. Cell 151:619-29. doi:
670 10.1016/j.cell.2012.09.017.

671 Neumann, S., and Schmid, S. L. (2013). Dual role of BAR domain-containing proteins in regulating vesicle
672 release catalyzed by the GTPase, dynamin-2. J Biol Chem. 288:25119-28. doi: 10.1074/jbc.M113.490474.

673 Niko, Y., Didier, P., Mely, Y., Konishi, G.-i., and Klymchenko, A. S. (2016). Bright and photostable push-pull
674 pyrene dye visualizes lipid order variation between plasma and intracellular membranes. Sci Rep. 6:18870.
675 doi: 10.1038/srep18870.

676 Olbrich, K., Rawicz, W., Needham, D., and Evans, E. (2000). Water permeability and mechanical strength of
677 polyunsaturated lipid bilayers. Biophys J 79:321-27.

678 Parinello, M. and Rahman, A. (1981). Polymorphic transitions in single crystals: A new molecular dynamics
679 method. J Applied Physics 52:7182-90. doi: 10.1063/1.328693

680 Pinot, M., Vanni, S., Pagnotta, S., Lacas-Gervais, S., Payet, L.-A., Ferreira, T., Gautier, R., Goud, B., Antonny,
681 B. Barelli, H. (2014). Polyunsaturated phospholipids facilitate membrane deformation and fission by
682 endocytic proteins. Science 345:693-7. doi: 10.1126/science.1255288.

683 Puchkov, D., and Haucke, V. (2013). Greasing the synaptic vesicle cycle by membrane lipids. Trends Cell Biol
684 23:493-503. doi: 10.1016/j.tcb.2013.05.002.

685 Qi, Y., Ingólfsson, H. I., Cheng, X., Lee, J., Marrink, S. J., and Im, W. (2015). CHARMM-GUI martini maker for
686 coarse-grained simulations with the martini force field. J Chem Theory Comput 11:4486-94. doi:
687 10.1021/acs.jctc.5b00513.

688 Rawicz, W., Olbrich, K., McIntosh, T., Needham, D., and Evans, E. (2000). Effect of chain length and
689 unsaturation on elasticity of lipid bilayers. Biophys J 79:328-39.

690 Rice, D. S., Calandria, J. M., Gordon, W. C., Jun, B., Zhou, Y., Gelfman, C. M., et al. (2015). Adiponectin
691 receptor 1 conserves docosahexaenoic acid and promotes photoreceptor cell survival. Nat Comms 6:6228.
692 doi: 10.1038/ncomms7228.

693 Rong, X., Wang, B., Dunham, M. M., Hedde, P. N., Wong, J. S., Gratton, E., et al. (2015). Lpcat3-dependent
694 production of arachidonoyl phospholipids is a key determinant of triglyceride secretion. Elife, 4.
695 doi:10.7554/eLife.06557.

696 Roux, A., Koster, G., Lenz, M., Sorre, B., Manneville, J.-B., Nassoy, P., et al. (2010). Membrane curvature
697 controls dynamin polymerization. Proc Natl Acad Sci U S A. 107:4141-6. doi: 10.1073/pnas.0913734107.

698 Shindou, H., Hishikawa, D., Harayama, T., Eto, M., and Shimizu, T. (2013). Generation of membrane diversity
699 by lysophospholipid acyltransferases. J Biochem 154:21-8. doi: 10.1093/jb/mvt048.

700 Simunovic, M., Manneville, J.-B., Renard, H.-F., Evergren, E., Raghunathan, K., Bhatia, D., et al. (2017).
701 Friction mediates scission of membrane nanotubes scaffolded by bar proteins. Cell 170:172-84. doi:
702 10.1016/j.cell.2017.05.047.

703 Slepnev, V. I., and De Camilli, P. (2000). Accessory factors in clathrin-dependent synaptic vesicle
704 endocytosis. Nat Rev Neurosci 1:161-72.

705 Stillwell, W., and Wassall, S. R. (2003). Docosahexaenoic acid: membrane properties of a unique fatty acid.
706 Chem Phys Lipids 126:1-27.

707 Stowell, M. H., Marks, B., Wigge, P., and McMahon, H. T. (1999). Nucleotide-dependent conformational
708 changes in dynamin: evidence for a mechanochemical molecular spring. Nat Cell Biol 1:27-32.

709 Sundborger, A., Soderblom, C., Vorontsova, O., Evergren, E., Hinshaw, J. E., and Shupliakov, O. (2011). An
710 endophilin–dynamin complex promotes budding of clathrin-coated vesicles during synaptic vesicle
711 recycling. J Cell Sci 124:133-43. doi: 10.1242/jcs.072686.

712 Takamori, S., Holt, M., Stenius, K., Lemke, E. A., Grønborg, M., Riedel, D., et al. (2006). Molecular anatomy
713 of a trafficking organelle. Cell 127:831-46.

714 Tam, O., and Innis, S. M. (2006). Dietary polyunsaturated fatty acids in gestation alter fetal cortical
715 phospholipids, fatty acids and phosphatidylserine synthesis. Dev Neurosci 28:222-9.

716 Tattrie, N. (1959). Positional distribution of saturated and unsaturated fatty acids on egg lecithin. J Lipid Res
717 1:60-5.

718 Vamparys, L., Gautier, R., Vanni, S., Bennett, W. D., Tieleman, D. P., Antonny, B., et al. (2013). Conical lipids
719 in flat bilayers induce packing defects similar to that induced by positive curvature. Biophysical J 104:585-
720 93. doi: 10.1016/j.bpj.2012.11.3836.

721 Wassenaar, T. A., Ingólfsson, H. I., Böckmann, R. A., Tieleman, D. P., and Marrink, S. J. (2015). Computational
722 lipidomics with insane: a versatile tool for generating custom membranes for molecular simulations. J Chem
723 Theory Comput 11:2144-55. doi: 10.1021/acs.jctc.5b00209.

724 Yabuuchi, H., and O'Brien, J. S. (1968). Positional distribution of fatty acids in glycerophosphatides of bovine
725 gray matter. J Lipid Res 9:65-67.

726 Yang, H.-J., Sugiura, Y., Ikegami, K., Konishi, Y., and Setou, M. (2012). Axonal gradient of arachidonic acid-
727 containing phosphatidylcholine and its dependence on actin dynamics. J Biol Chem 287:5290-5300. doi:
728 10.1074/jbc.M111.316877.

729 Zeng, Y., Han, X., and Gross, R. W. (1998). Phospholipid subclass specific alterations in the passive ion
730 permeability of membrane bilayers: separation of enthalpic and entropic contributions to transbilayer ion
731 flux. Biochemistry 37:2346–2355.

732

733

734 **FIGURE LEGENDS**

735 **Figure 1. GTPase activity of dynamin on liposomes made of phospholipids with different combinations of**
736 **acyl chains. A**. Principle of the experiments and chemical structure of the various phospholipid species
737 used in this study. **B**. Rate of GTP hydrolysis by dynamin (0.3 µM) ± endophilin (0.6 µM) with large
738 liposomes (400 nm extrusion) containing phospholipids with symmetric (green) or asymmetric (red) acyl
739 chains at positions *sn1* and *sn2* as shown in A. Data are mean ± SD from three independent experiments. All
740 lipid compositions are detailed in Table S1. **C**. Electron microscopy analysis of 22:6-22:6 or 18:0-22:6
741 liposomes after incubation with dynamin (0.5 µM) and with GTP or GTPγS. With GTPγS, numerous dynamin
742 spirals formed on 22:6-22:6 liposomes but not on 18:0-22:6 liposomes. With GTP, almost all 22:6-22:6
743 liposomes were transformed into very small (radius < 20 nm) structures, whereas large parental profiles
744 were still abundant in the case of 18:0-22:6 liposomes. Scale bar, 200 nm.

745 **Figure 1-figure supplement 1**. **A**. Time course of GTP hydrolysis by dynamin (0.3 µM) with large liposomes
746 (400-nm extrusion) containing phospholipids with asymmetric (left panel) or symmetric (right panel) acyl
747 chains at positions sn-1 and sn-2 as shown in Figure 1A. **B**. Electron microscopy analysis of 22:6-22:6 or
748 18:0-22:6 liposomes after incubation with dynamin and with GTP or GTPγS. With GTPγS, numerous dynamin
749 spirals formed and tubulated 22:6-22:6 liposomes but not in the presence of 18:0-22:6 liposomes. With
750 GTP, dynamin extensively vesiculated 22:6-22:6 liposomes into very small (radius < 20 nm) structures,
751 whereas large parental profiles were still abundant in the case of 18:0-22:6 liposomes. Scale bar, 500 nm.
752 All lipid compositions are shown in Table S1.

753 **Figure 2. Membranes with symmetrical but not asymmetrical polyunsaturated phospholipids are highly**
754 **permeable. A**. Left: snapshot of a lipid bilayer with the same composition as that used in the dynamin
755 GTPase assay. The red circle highlights a water molecule in the membrane hydrophobic region. Right: % of
756 water molecules visiting the membrane hydrophobic region during a 100 ns simulation as a function of
757 phospholipid acyl chain composition. **B**. Hydratation of the interfacial region of the same liposomes as that
758 used in Figure 1 as measured by the fluorescence of the push-pull pyrene dye PA. Left: typical emission
759 fluorescence spectra. Right: emission wavelength as a function of phospholipid acyl chain composition. **C**.
760 Dithionite-mediated NBD quenching assay. At t = 30 s, dithionite was added to the same liposomes as that
761 used in the GTPase assay but also containing PE-NBD. The dotted line indicates 50% of quenching, which is
762 the expected value if only externally orientated PE-NBD molecules are quenched by dithionite. At t = 350 s,
763 0.1% Triton X-100 was added to allow the quenching of all PE-NBD molecules. Data on the right bar plot are
764 mean ± variation from two independent experiments. **D**. GUVs permeability measurements. GUVs
765 containing the 55 mol % of the indicated polyunsaturated phospholipids were incubated with soluble
766 Alexa488 and imaged by confocal microscopy. Data show all GUVs measured from six independent

767 experiments and from two independent GUV preparations (large horizontal bar: mean; vertical bar SD). All
768 lipid compositions are detailed in Table S1, S2 and S4.

769 **Figure 2-figure supplement 1**. Emission fluorescence spectrum of the push-pull pyrene dye PA in the
770 presence of the same liposomes as that used in Figure 1 to determine the hydratation of the membrane
771 interfacial region. All lipid compositions are shown in Table S1.

772 **Figure 3. Higher activity of dynamin on liposomes containing 18:0-22:6 phospholipids as compared to**
773 **other polyunsaturated phospholipids.** GTPase activity of dynamin (0.3 µM) in the presence of endophilin
774 (0.6 µM) and with large liposomes (400-nm extrusion) containing increasing amounts of the indicated
775 asymmetric polyunsaturated phospholipids at the expense of 18:0-18:1 phospholipids. Data are mean ± SD
776 from three independent experiments. All lipid compositions are shown in Table S1.

777 **Figure 3-figure supplement 1. A**. GTPase rate of dynamin (0.3 µM) ± endophilin (0.6 µM) with large
778 liposomes (400-nm extrusion) containing PS, PE, and PC with the indicated acyl chains, cholesterol and
779 supplemented with 0 to 5% $PIP_2$ at the expense of PC (see Table S3 for the exact lipid composition). **B**.
780 GTPase rate of dynamin (0.3 µM) in the absence of in the presence of endophilin (0.6 µM) or SNX9 (0.6 µM)
781 and with liposomes of fixed polar head composition but different acyl chain profiles.

782 **Figure 4. Higher vesiculation activity of dynamin and endophilin on liposomes containing 18:0-22:6**
783 **phospholipids compared to 18:0-20:4 phospholipids. A**. Electron micrographs of 18:0-18:1, 18:0-20:4 and
784 18:0-22:6 liposomes (400-nm extrusion) before or after incubation with dynamin (0.5 µM), endophilin (1
785 µM), and GTP or GTPγS (500 µM). Scale bar, 500 nm. **B-C**. Quantification of membrane tubulation (B) and
786 vesiculation (C) from three independent experiments similar to that shown in A. In B, the tube radius and
787 the protein spiral pitch was determined after 5 or 15 min incubations of the liposomes with dynamin,
788 endophilin and GTPγ (see also Fig S4). In C, the size distribution of the membrane profiles was determined
789 after 30 min incubation of the liposomes with dynamin, endophilin and GTP. All lipid compositions are
790 showed in Table S1.

791 **Figure 4-figure supplement 1**. **A**. Illustration of the measurements used to quantify the effect of dynamin
792 and endophilin on liposomes in TEM experiments. These include the tube radius, the pitch of the
793 dynamin+endophilin spiral and the size of the circular profiles. **B**. Electron micrographs of C18:0-C20:4 or
794 C18:0-C22:6 liposomes (400-nmextrusion) after 15 min incubation with dynamin (0.5 µM), endophilin (1
795 µM), and GTP or GTPγS (500 µM) at room temperature. Black arrows show membrane constructions; white
796 arrows show tube breakages. Scale bar, 200 nm. All lipid compositions are shown in Table S1.

797

798 **Figure 5. GUV shrinkage assay.** GUVs containing 18:0-20:4 or 18:0-22:6 phospholipids were incubated with
799 dynamin (0.5 µM) and endophilin (1 µM) in presence of GTP (500 µM) for 60 min at 37°C. **A**. Colored images
800 showing overlays of the GUVs at time 0 (red) and after 60 min incubation (green). Note the collapse of the
801 GUV containing 18:0-22:6 after 60 min incubation with the protein-nucleotide mixture. **B-C**. Quantification
802 of the experiment shown in (A) showing the GUV shrinking distribution after 60 min and mean ±SD over the
803 time. Data are obtained from ~100 GUVs from five independent preparations. All lipid compositions are
804 showed in Table S4.

805 **Figure 5-figure supplement 1.** GUVs containing the indicated amounts of C18:0-C18:1 were incubated with
806 dynamin (0.5 µM) and endophilin (1 µM) in presence of GTP (500 µM) for 60 min at 37°C. A. The colored
807 images show overlays of the GUVs at time 0 (red) and after 60 min incubation (green). No significant effect
808 was detected on these GUVs as compared to GUVs with polyunsaturated phospholipids (see Figure 5). **B-C.**
809 Quantification of the experiment shown in (A) showing the GUV shrinking distribution after 60 min and
810 mean ±SD over the time. Data are obtained from ~20 GUVs from one preparation. Lipid composition is
811 shown in Table S4.

812 **Figure 6: Molecular dynamics simulations. A**. Top: snapshots at t = 200 ns of tubes as pulled with a 200 KJ
813 $mol^{-1}$ $nm^{-1}$ force from coarse-grained models of membranes with the indicated asymmetric polyunsaturated
814 PC. Bottom: plot of *L/R* as a function of the pulling force. The tube geometry was analyzed at t = 200 ns. **B**.
815 Top: snapshots of a tube pulling coarse-grained simulation (Force = 250 KJ $mol^{-1}$ $nm^{-1}$) obtained from a
816 membrane with 18:0-20:4 PC and showing elongation and fission. See also **video 1**. Bottom: summary of all
817 simulations. Elongation, fission (F) and breakage events (B) are indicated. In contrast to fission, a breakage
818 event corresponds to a rupture at the level of the lipids where the pulling force is applied. **C-F**. Dynamics of
819 the acyl chains of asymmetric polyunsaturated phospholipids from all-atom simulations. The analysis was
820 performed on flat membrane patches with the same composition as that used in the experiments. **C**.
821 Velocity rate of the terminal $CH_3$ group of the acyl chain along either the membrane normal (*z* velocity) or in
822 the membrane plane (*x-y* velocity). **D**. Frequency of acyl chain torsions as defined as conformations for
823 which the acyl chain displays an angle < 100°. **E**. Number of protrusions of the $CH_3$ group above the glycerol
824 group of phospholipids. Color code for coarse-grained simulations: grey: lipid polar head and glycerol;
825 orange: acyl chain regions with double carbon bonds; yellow: acyl chain regions with single carbon bonds.
826 Color code for all-atom simulations: Grey: lipid polar head; cyan: glycerol; yellow: *sn1* or *sn2* acyl chains.

827 **Figure 6-figure supplement 1**. **A**. Comparison of an authentic fission event and a breakage event. In the first
828 case, the membrane divides below the phospholipid patch (red) that endures the pulling force. In the
829 second case, the membrane divides within the phospholipid patch (red) that endures the pulling force **B**.
830 Time course of tube pulling from coarse-grained models of membranes with asymmetric polyunsaturated

831 phospholipids. Traces ending before 200 ns correspond to tubes that underwent breakage (B) or fission (F).
832 See also Figure 6A-B.

833 **Figure 6-figure supplement 2**. Distribution of deep and shallow lipid packing defects in all-atom simulations
834 of membranes with the same composition as that used in the experiments of Figure 1 and detailed in Table
835 S1.

836 **Figure 6-figure supplement 3**. Comparison of phospholipids with a natural *sn1*-saturated-*sn2*-
837 polyunsaturated profile and with a swapped *sn1*-polysaturated-*sn2*-saturated profile. **A.** Velocity rate of the
838 terminal $CH_3$ group of the acyl chains along the membrane normal (*z* velocity). For comparison, the values
839 shown in Figure 6 for natural phospholipids have been reported. **B.** Density profile of the acyl chains across
840 the membrane bilayer. Also shown are the density profiles of the phosphate group, which were used to
841 estimate the bilayer thickness. **C.** Summary of the membrane tether pulling simulations. See also **video 2**.

842 **Video 1.** Simulation of the formation of a tubule and its subsequent fission from a coarse-grained model of
843 a membrane containing 18:0-20:4 phospholipids (see also Figure 6B) and submitted to a pulling force of 250
844 KJ $mol^{-1}$ $nm^{-1}$.

845 **Video 2.** Simulation of the formation of a tubule and its subsequent fission from a coarse-grained bilayer
846 containing 18:0-22:6 or 22:6-18:0 phospholipids (see also Figure 6-supplement figure 3C) and submitted to
847 a pulling force of 200 KJ $mol^{-1}$ $nm^{-1}$. The 22:6-18:0 tubule is thinner and fissions before the 18:0-22:6 tubule.

848 **Supplementary file 1.** Tables of the lipid composition of the various bilayers used in this study.

849 **Supplementary file 2.** Mdp input file of the all atom simulations.

850 **Supplementary file 3.** Mdp input file of the coarse-grained simulations

851

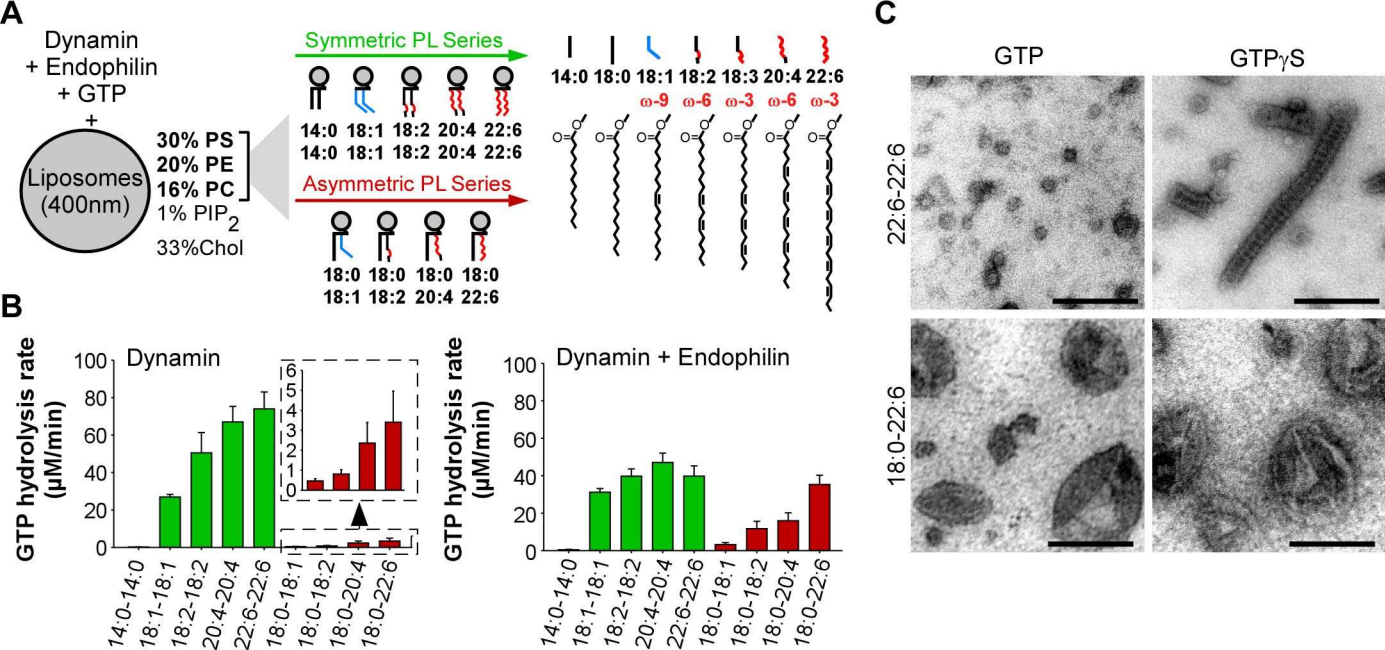
A
Dynamin
+ Endophilin
+ GTP
+
Liposomes
(400nm)
30% PS
20% PE
16% PC
1% PIP2
33%Chol
Symmetric PL Series
14:0 18:1 18:2 20:4 22:6
14:0 18:1 18:2 20:4 22:6
Asymmetric PL Series
18:0 18:0 18:0 18:0
18:1 18:2 20:4 22:6
14:0 18:0 18:1 18:2 18:3 20:4 22:6
ω-9 ω-6 ω-3 ω-6 ω-3
B
Dynamin
GTP hydrolysis rate
(μM/min)
14:0-14:0
18:1-18:1
18:2-18:2
20:4-20:4
22:6-22:6
18:0-18:1
18:0-18:2
18:0-20:4
18:0-22:6
Dynamin + Endophilin
C
GTP
GTPγS
22:6-22:6
18:0-22:6

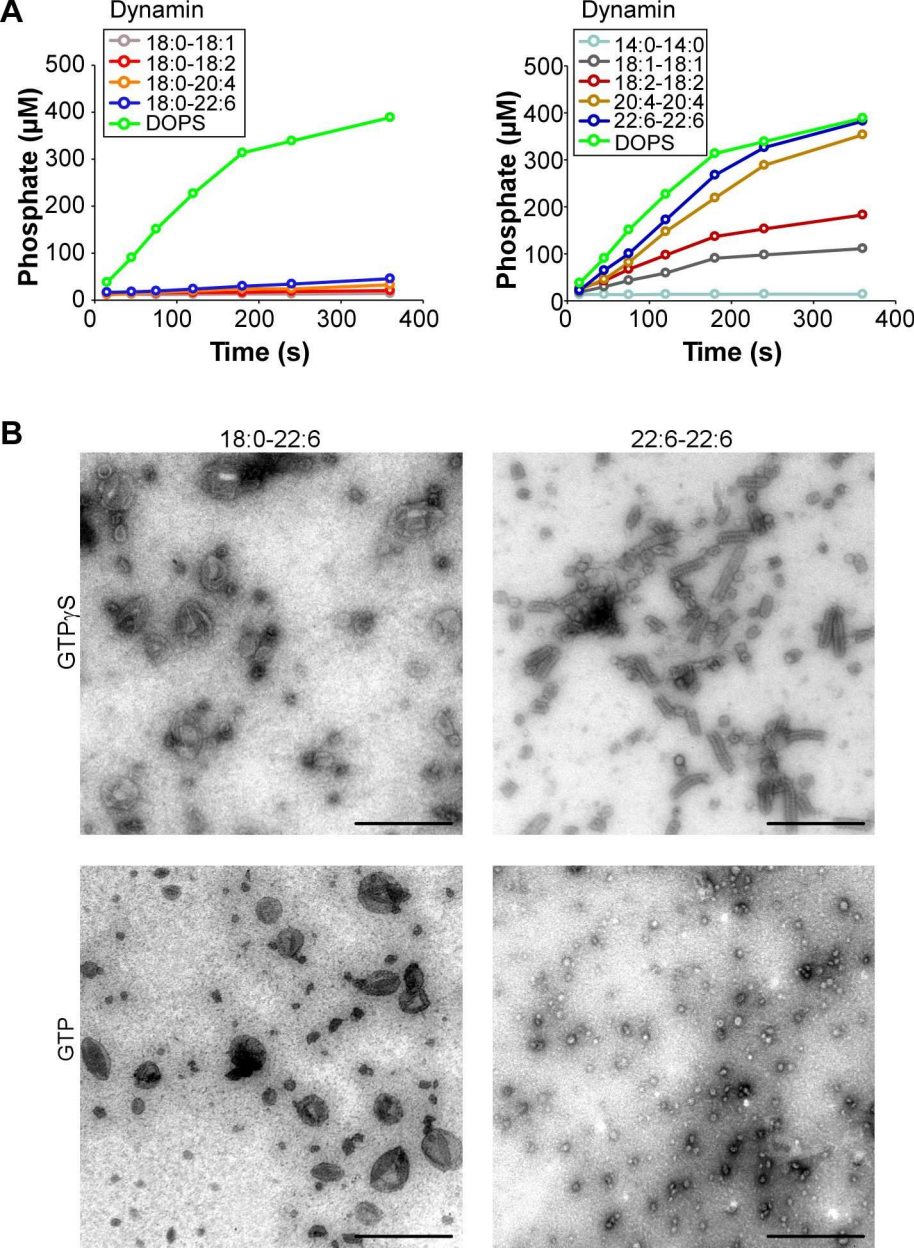
A
Dynamin
18:0-18:1
18:0-18:2
18:0-20:4
18:0-22:6
DOPS
Phosphate (μM)
Time (s)
Dynamin
14:0-14:0
18:1-18:1
18:2-18:2
20:4-20:4
22:6-22:6
DOPS
Phosphate (μM)
Time (s)
B
18:0-22:6
22:6-22:6
GTPγS
GTP

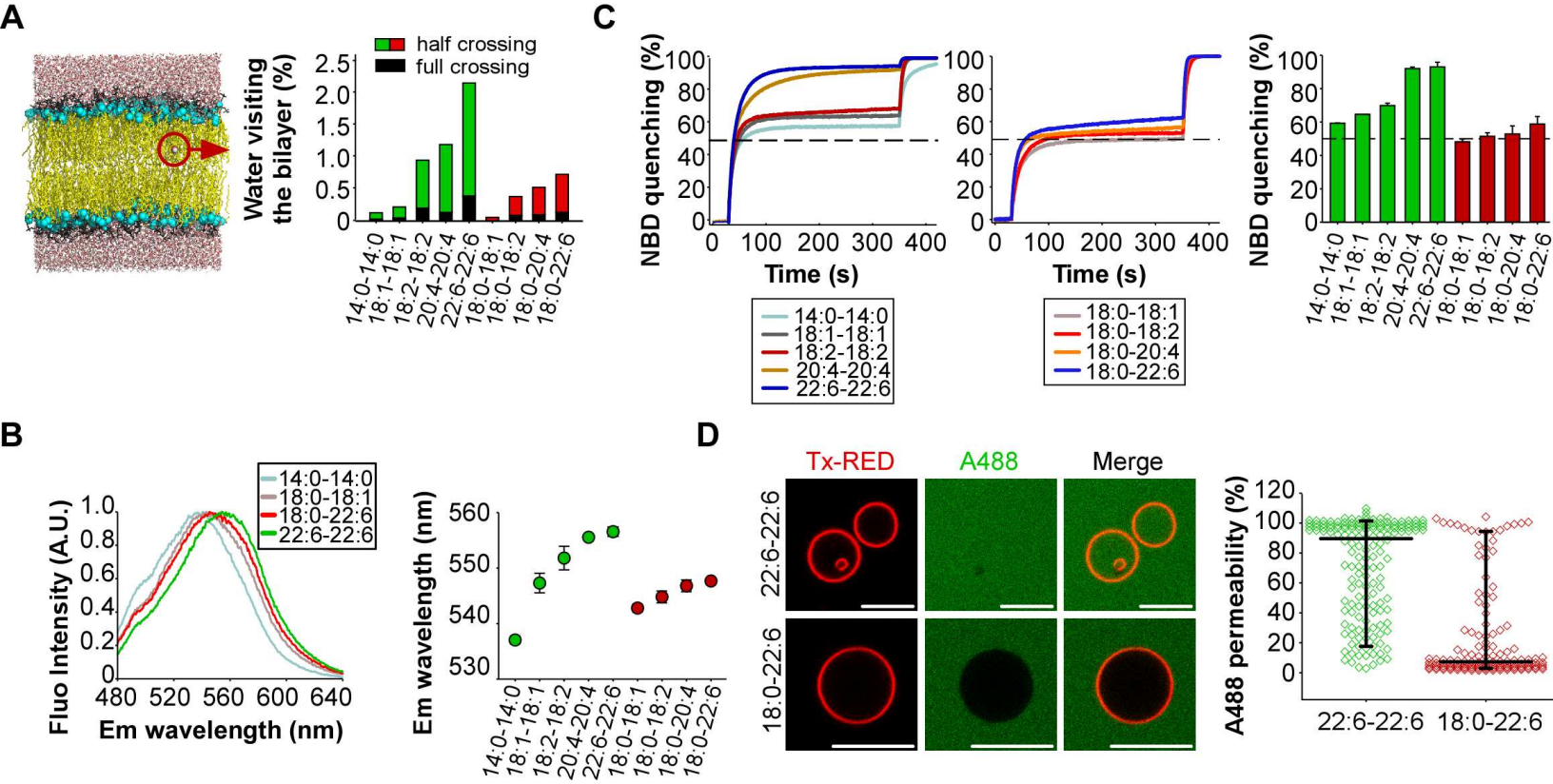
A
half crossing
full crossing
Water visiting the bilayer (%)
2.5
2.0
1.5
1.0
0.5
0
14:0-14:0
18:1-18:1
18:2-18:2
20:4-20:4
22:6-22:6
18:0-18:1
18:0-18:2
18:0-20:4
18:0-22:6
C
NBD quenching (%)
100
80
60
40
20
0
0 100 200 300 400
Time (s)
14:0-14:0
18:1-18:1
18:2-18:2
20:4-20:4
22:6-22:6
18:0-18:1
18:0-18:2
18:0-20:4
18:0-22:6
B
Fluo Intensity (A.U.)
1.0
0.8
0.6
0.4
0.2
0
480 520 560 600 640
Em wavelength (nm)
Em wavelength (nm)
560
550
540
530
D
Tx-RED
A488
Merge
22:6-22:6
18:0-22:6
A488 permeability (%)
120
100
80
60
40
20
0
22:6-22:6
18:0-22:6

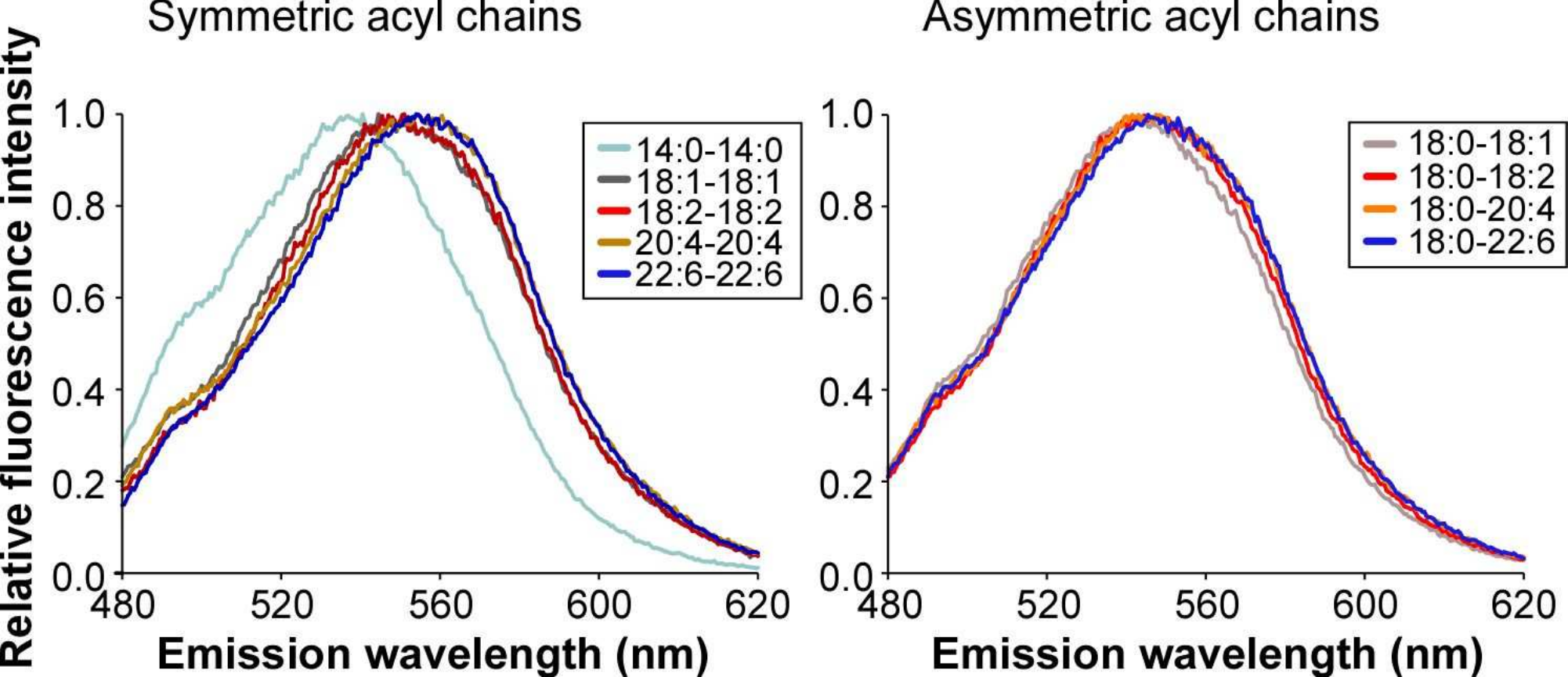
Symmetric acyl chains
Asymmetric acyl chains
Relative fluorescence intensity
1.0
0.8
0.6
0.4
0.2
0.0
480
520
560
600
620
Emission wavelength (nm)
14:0-14:0
18:1-18:1
18:2-18:2
20:4-20:4
22:6-22:6
18:0-18:1
18:0-18:2
18:0-20:4
18:0-22:6

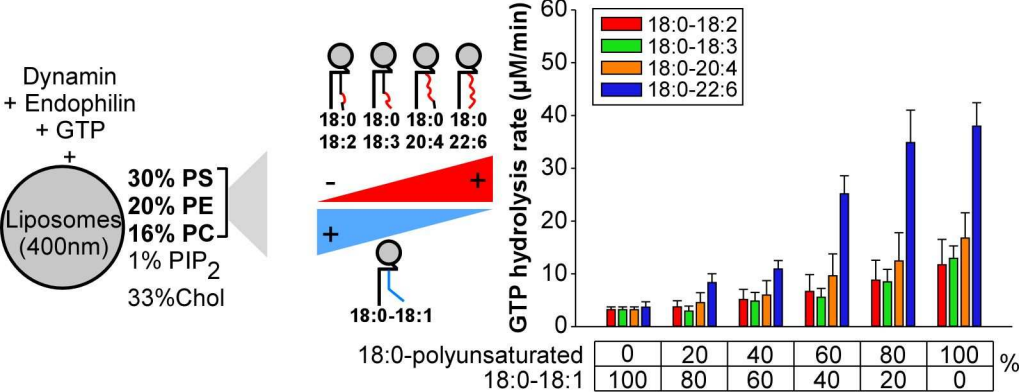
Dynamin
+ Endophilin
+ GTP
+
Liposomes
(400nm)
30% PS
20% PE
16% PC
1% PIP2
33%Chol
18:0 18:0 18:0 18:0
18:2 18:3 20:4 22:6
-
+
+
18:0-18:1
GTP hydrolysis rate (μM/min)
18:0-18:2
18:0-18:3
18:0-20:4
18:0-22:6
0
10
20
30
40
50
60
18:0-polyunsaturated 0 20 40 60 80 100 %
18:0-18:1 100 80 60 40 20 0

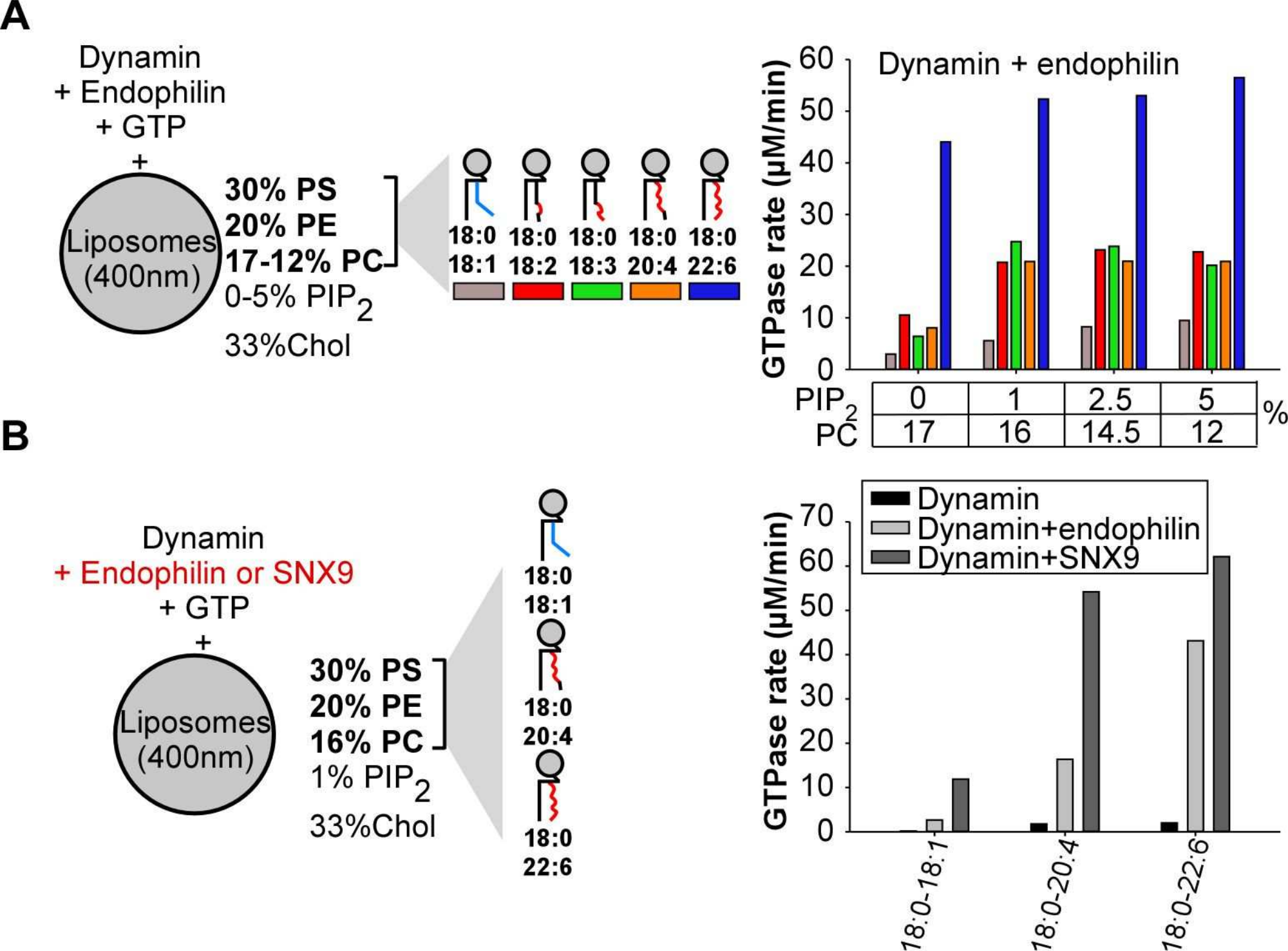
A
Dynamin
+ Endophilin
+ GTP
+
Liposomes
(400nm)
30% PS
20% PE
17-12% PC
0-5% PIP2
33%Chol
18:0
18:1
18:0
18:2
18:0
18:3
18:0
20:4
18:0
22:6
Dynamin + endophilin
GTPase rate (μM/min)
60
50
40
30
20
10
0
PIP2
0
1
2.5
5
%
PC
17
16
14.5
12
B
Dynamin
+ Endophilin or SNX9
+ GTP
+
Liposomes
(400nm)
30% PS
20% PE
16% PC
1% PIP2
33%Chol
18:0
18:1
18:0
20:4
18:0
22:6
Dynamin
Dynamin+endophilin
Dynamin+SNX9
GTPase rate (μM/min)
70
60
50
40
30
20
10
0
18:0-18:1
18:0-20:4
18:0-22:6

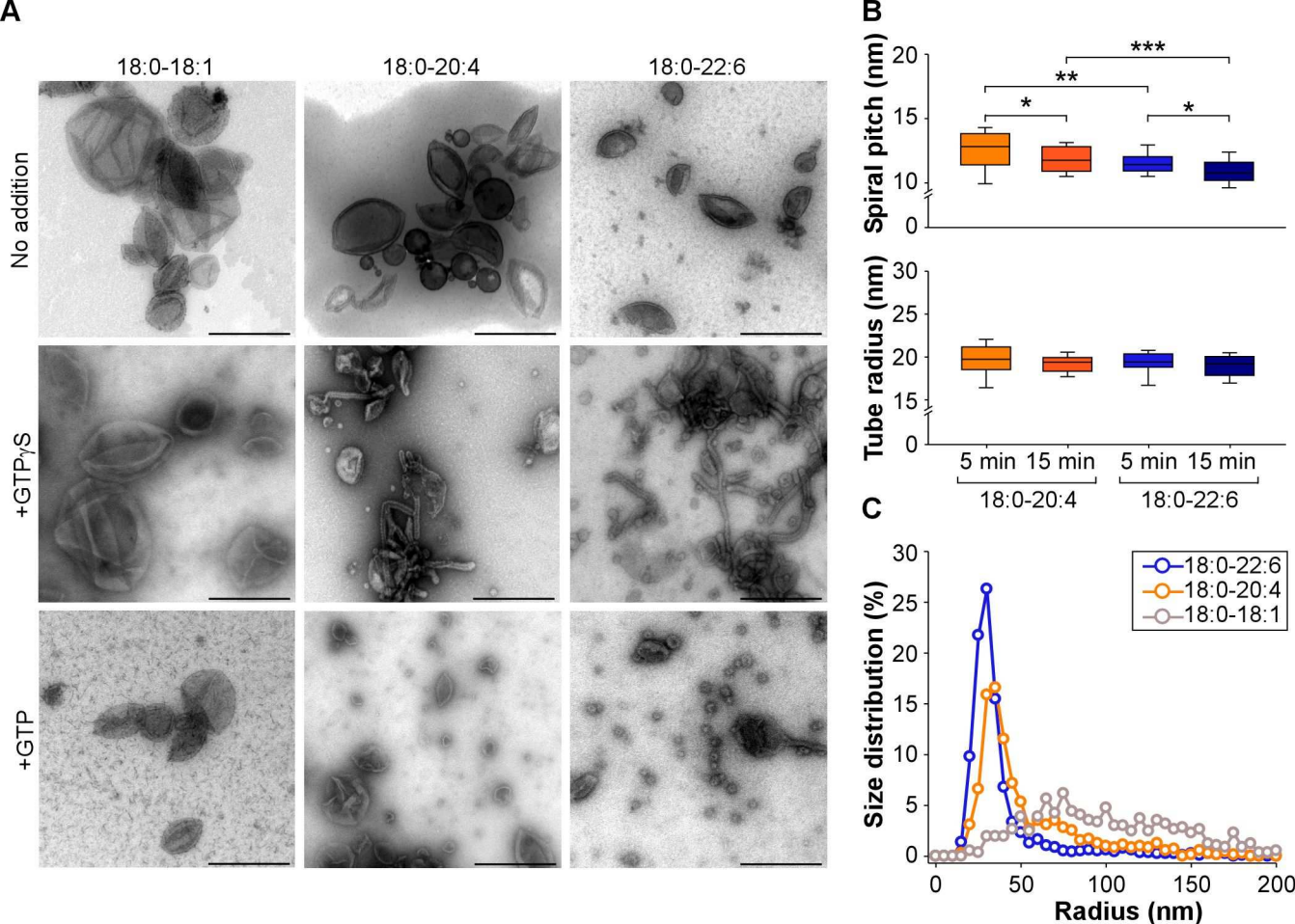
A
18:0-18:1
18:0-20:4
18:0-22:6
No addition
+GTPγS
+GTP
B
Spiral pitch (nm)
20
15
10
0
***
**
*
*
Tube radius (nm)
30
25
20
15
0
5 min
15 min
5 min
15 min
18:0-20:4
18:0-22:6
C
Size distribution (%)
30
25
20
15
10
5
0
18:0-22:6
18:0-20:4
18:0-18:1
0
50
100
150
200
Radius (nm)

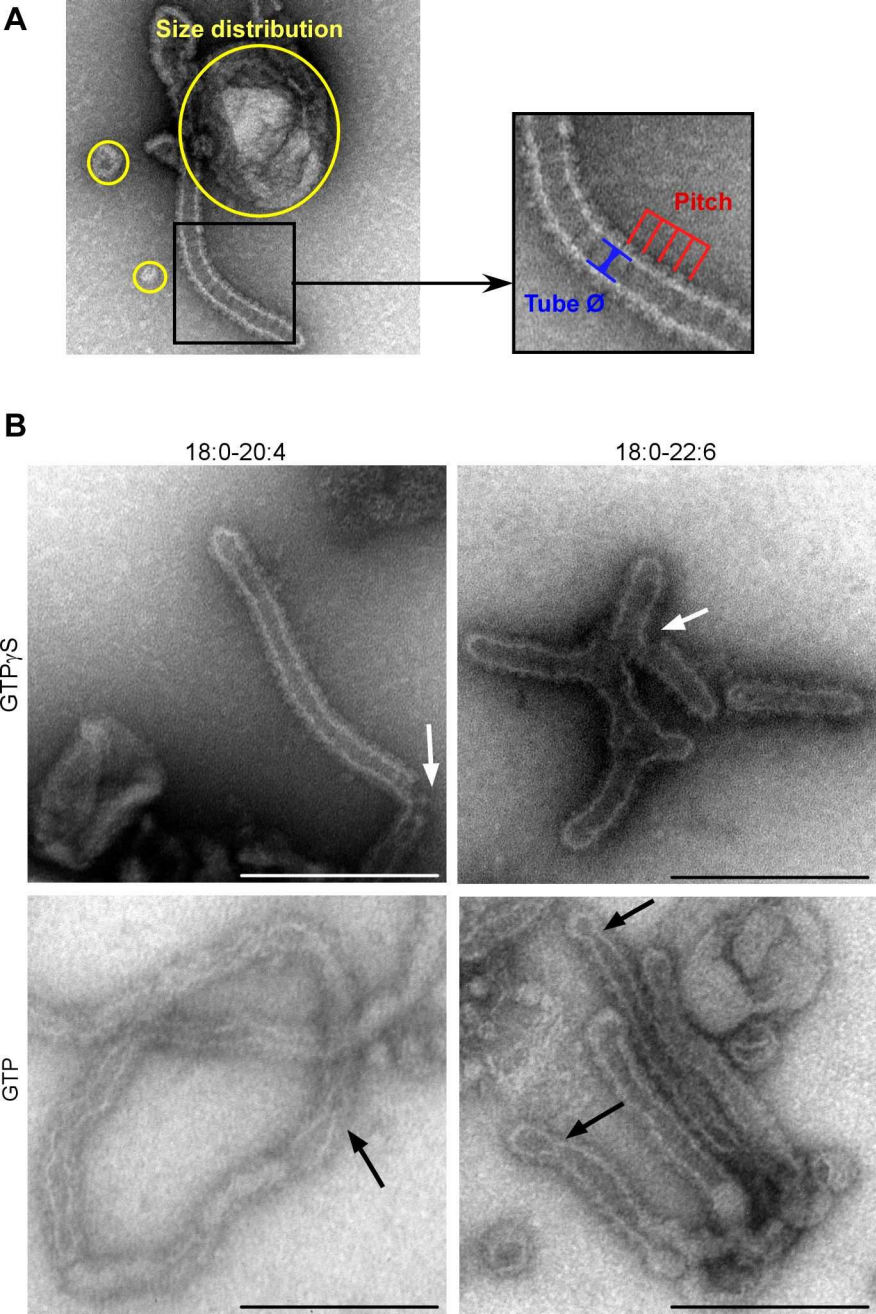
A
Size distribution
Pitch
Tube Ø
B
18:0-20:4
18:0-22:6
GTPγS
GTP

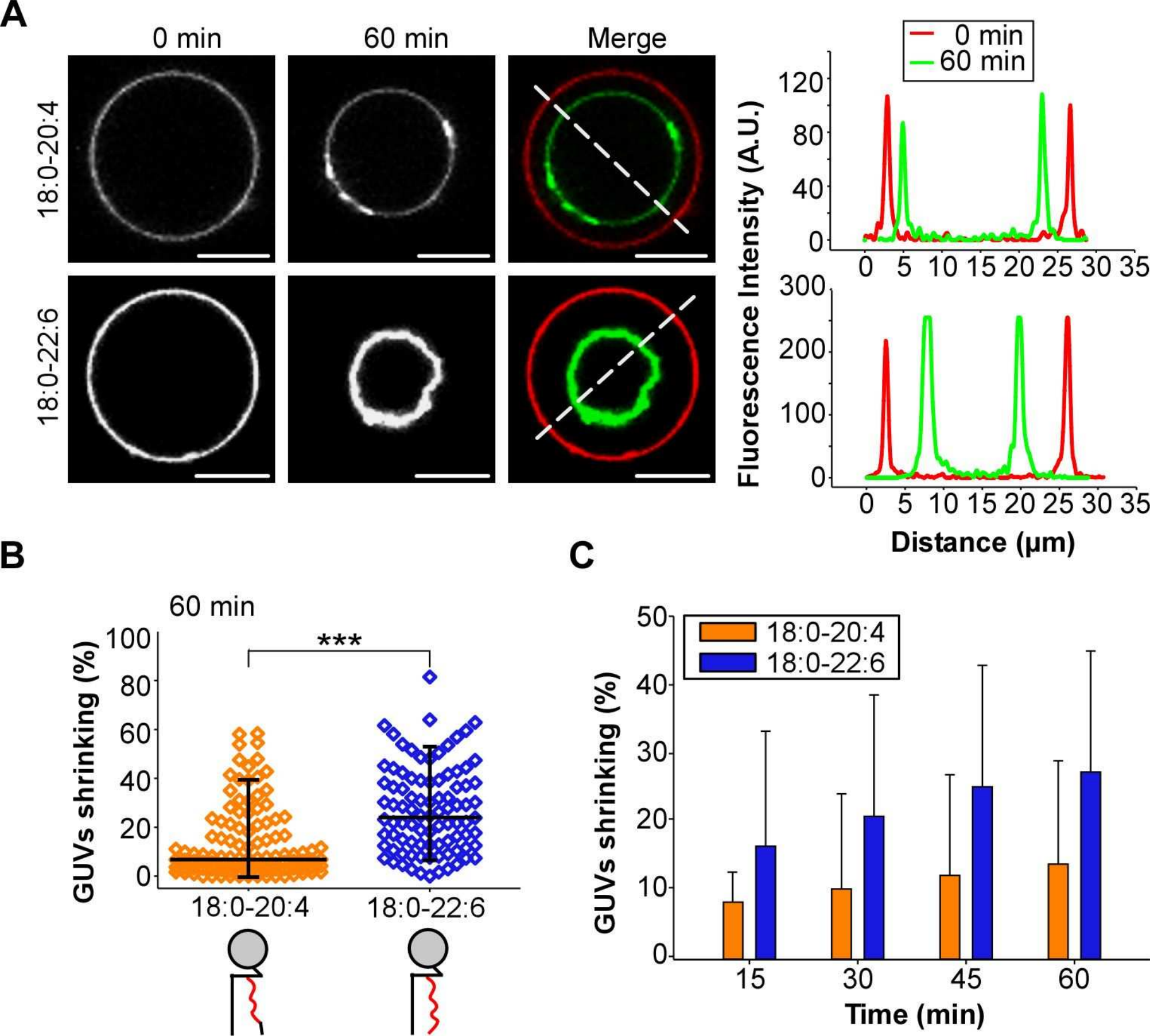
A
0 min
60 min
Merge
18:0-20:4
18:0-22:6
0 min
60 min
Fluorescence Intensity (A.U.)
Distance (µm)
B
60 min
***
GUVs shrinking (%)
18:0-20:4
18:0-22:6
C
18:0-20:4
18:0-22:6
GUVs shrinking (%)
Time (min)

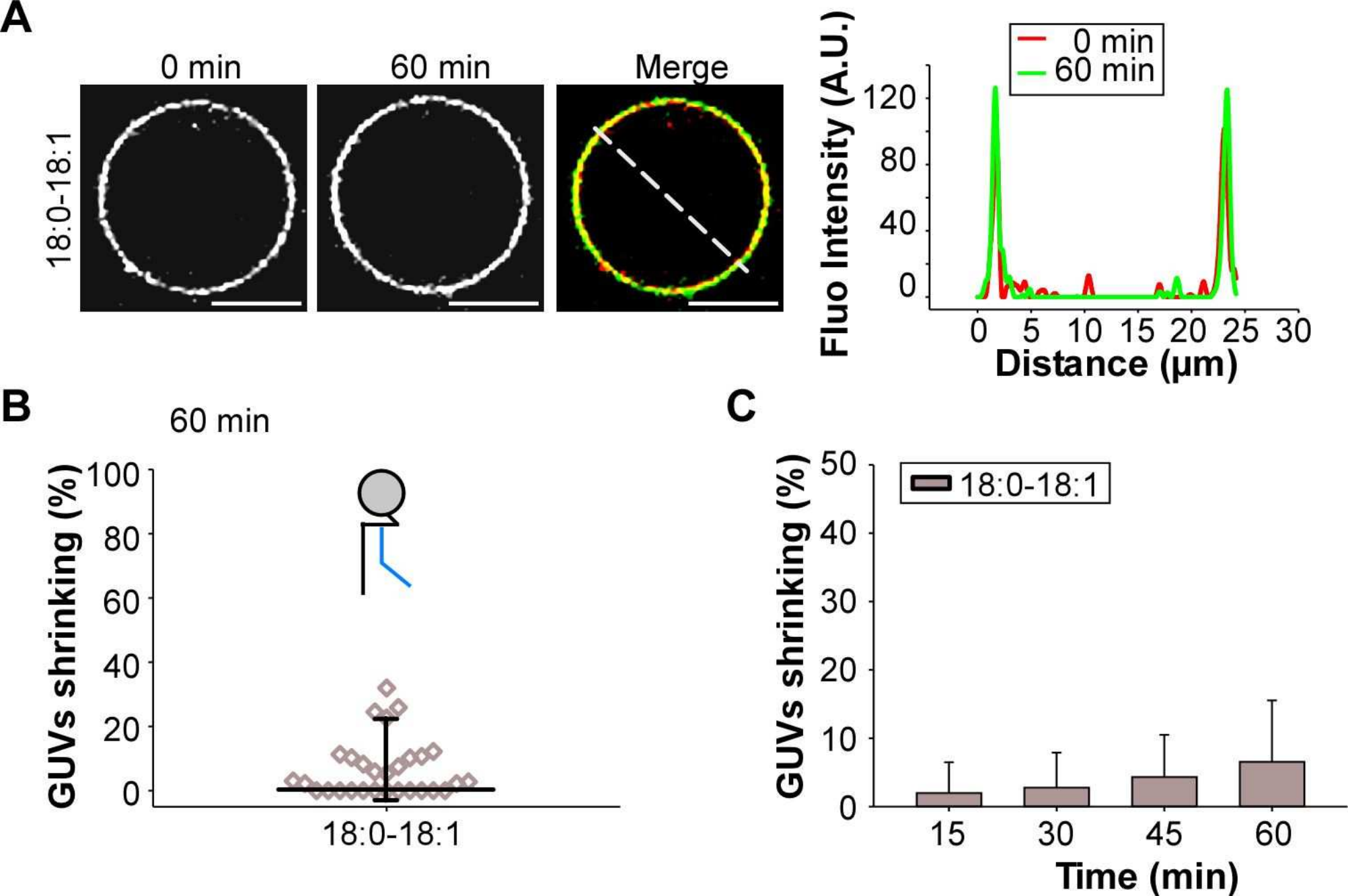
A
0 min
60 min
Merge
18:0-18:1
0 min
60 min
Fluo Intensity (A.U.)
120
80
40
0
0 5 10 15 20 25 30
Distance (µm)
B
60 min
GUVs shrinking (%)
100
80
60
40
20
0
18:0-18:1
C
18:0-18:1
GUVs shrinking (%)
50
40
30
20
10
0
15 30 45 60
Time (min)

## Coarse-grained simulations

**A**

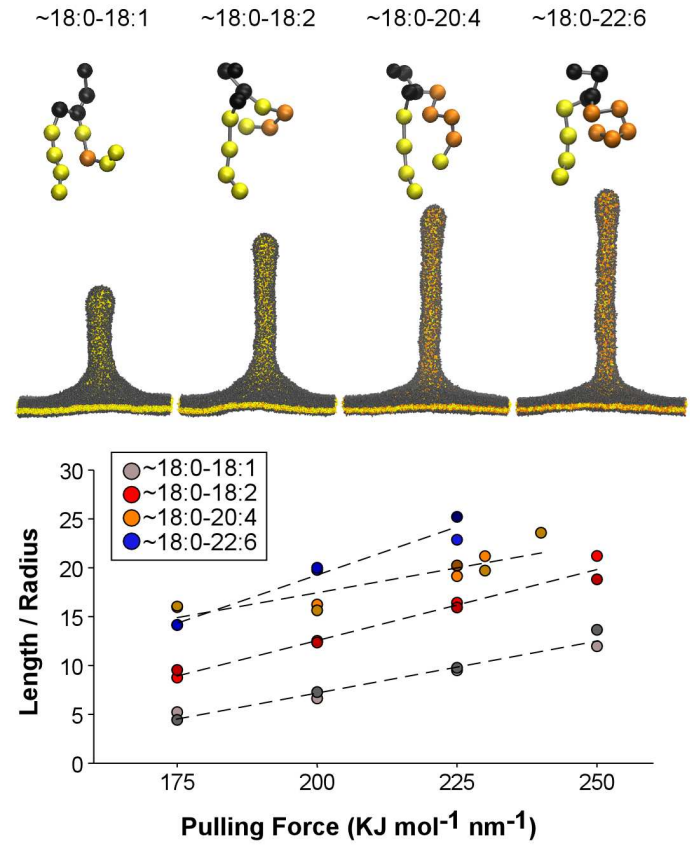


**B**

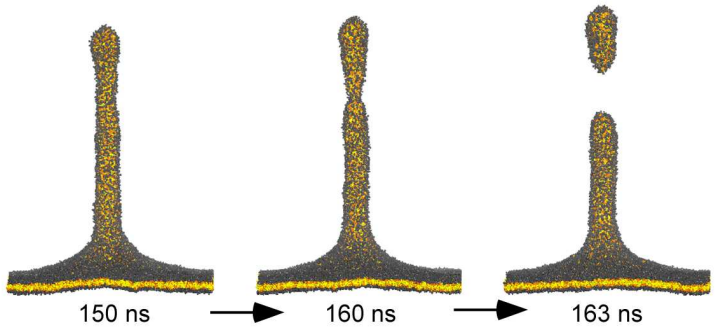


| Force | | ~18:0-18:1 | | ~18:0-18:2 | | ~18:0-20:4 | | ~18:0-22:6 | |
|---|---|---|---|---|---|---|---|---|---|
| KJ mol$^{-1}$ nm$^{-1}$ | pN | | | | | | | | |
| 175 | 290 | X | X | X | X | X | X | X | X |
| 200 | 332 | X | X | X | X | X | X | X | X |
| 225 | 373 | X | X | X | X | X X | X | X X | F(100ns) |
| 230 | 382 | | | | | X | X | B(101ns) | F(143ns) |
| 240 | 398 | | | | | X | F(194ns) | F(145ns) | F(100ns) |
| 250 | 415 | X | X | X | X | F(163ns) | F(197ns) | B(49ns) | B(55ns) |

X = Elongation
F = Fission
B = Breakage

## All-atom simulations

**C**

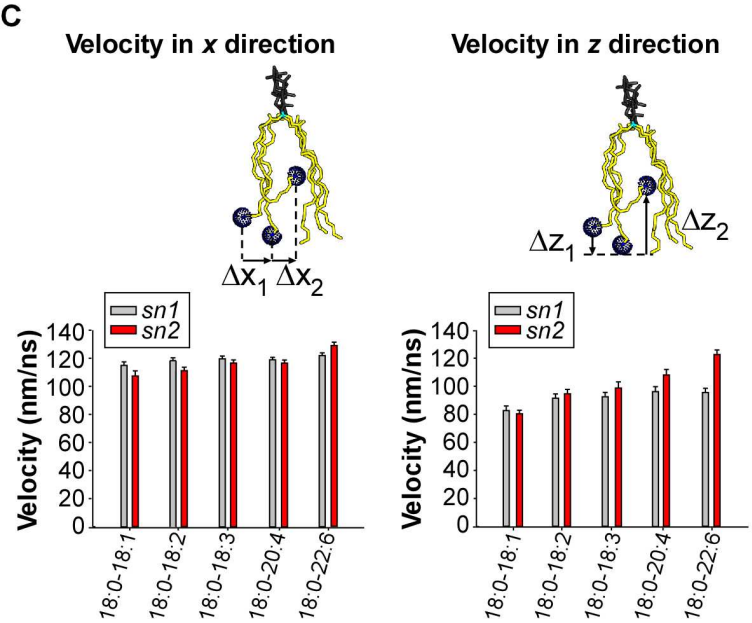


**D**

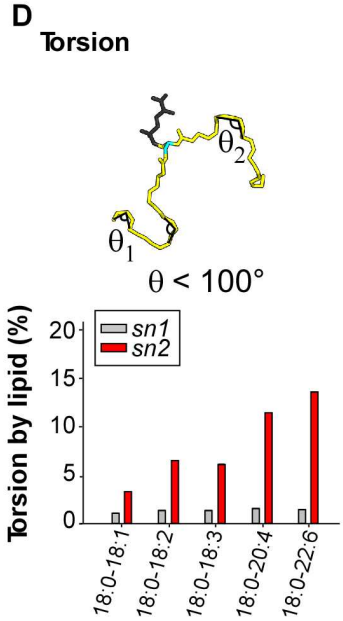


**E**

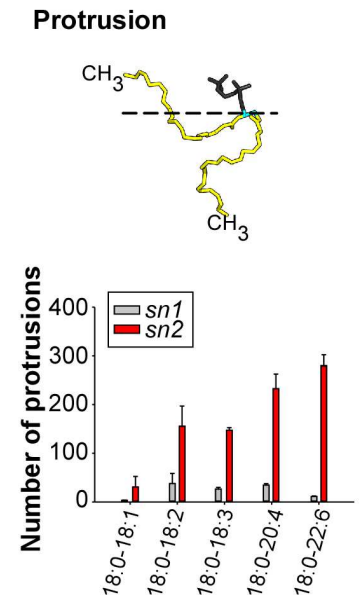

A

~18:0-22:6
F = 225 KJ mol$^{-1}$ nm$^{-1}$

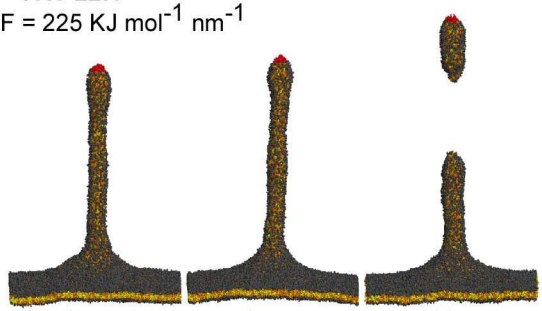


~18:0-22:6
F = 250 KJ mol$^{-1}$ nm$^{-1}$

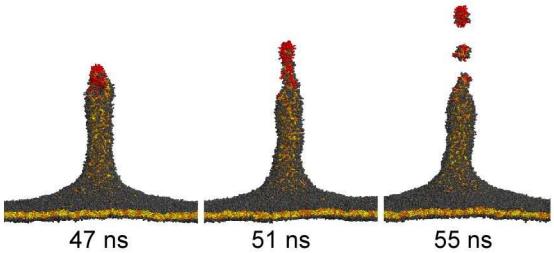


B

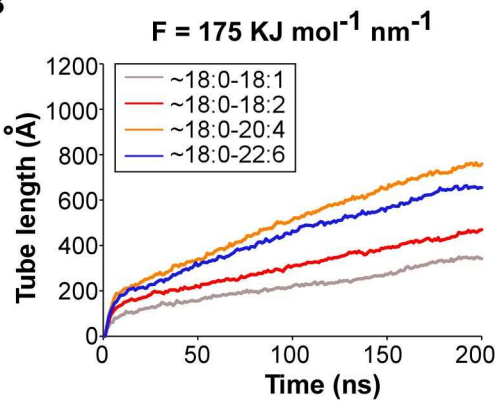


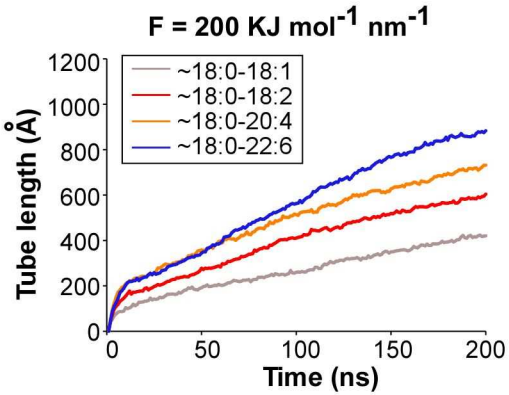


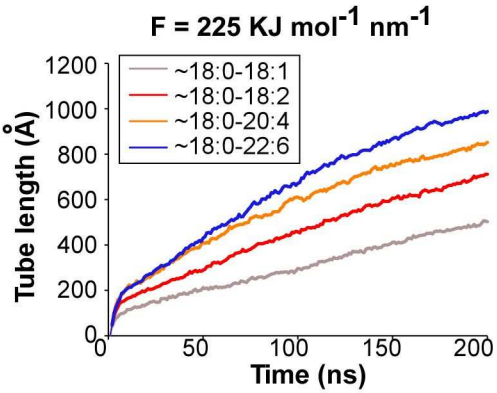


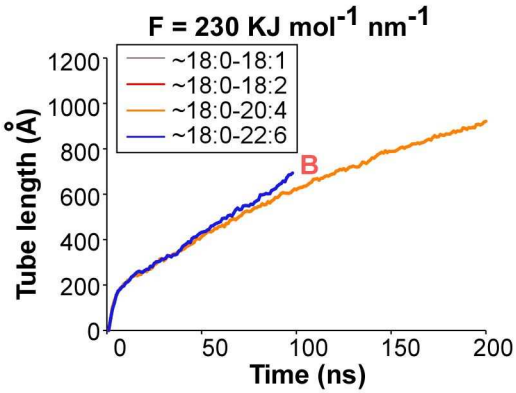


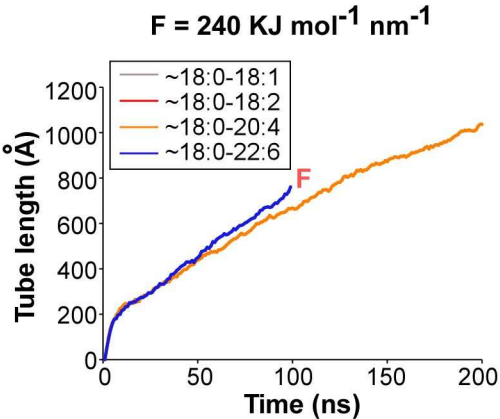


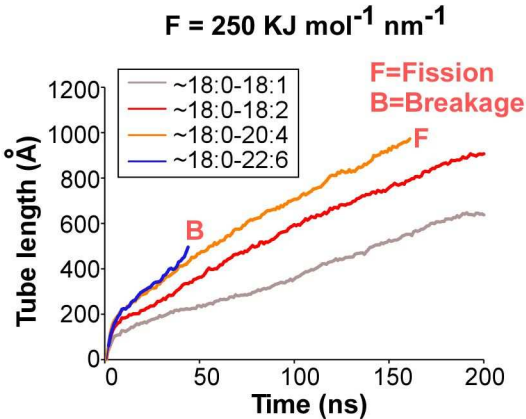

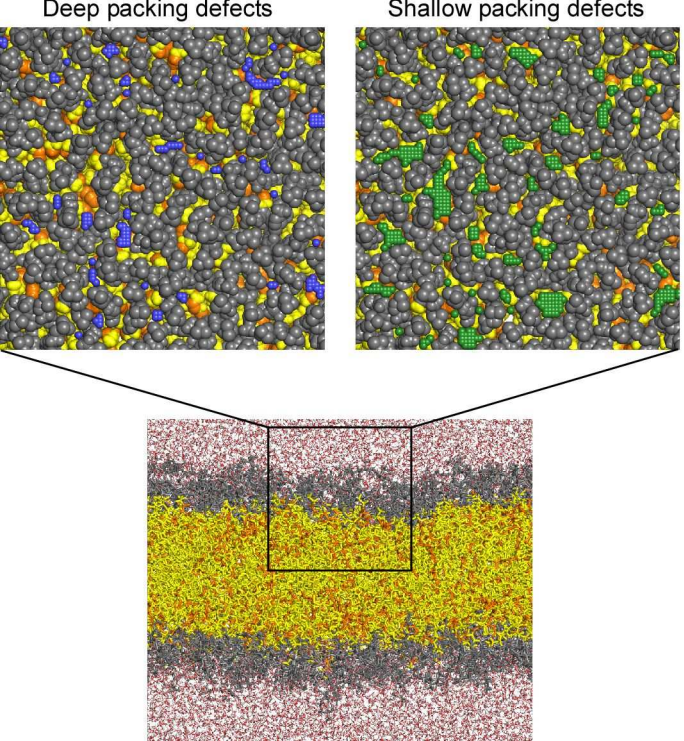
Deep packing defects
Shallow packing defects

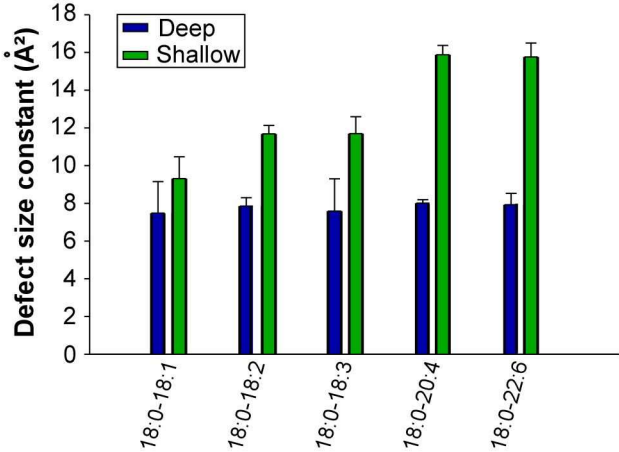
Defect size constant (Å²)
0
2
4
6
8
10
12
14
16
18
Deep
Shallow
18:0-18:1
18:0-18:2
18:0-18:3
18:0-20:4
18:0-22:6

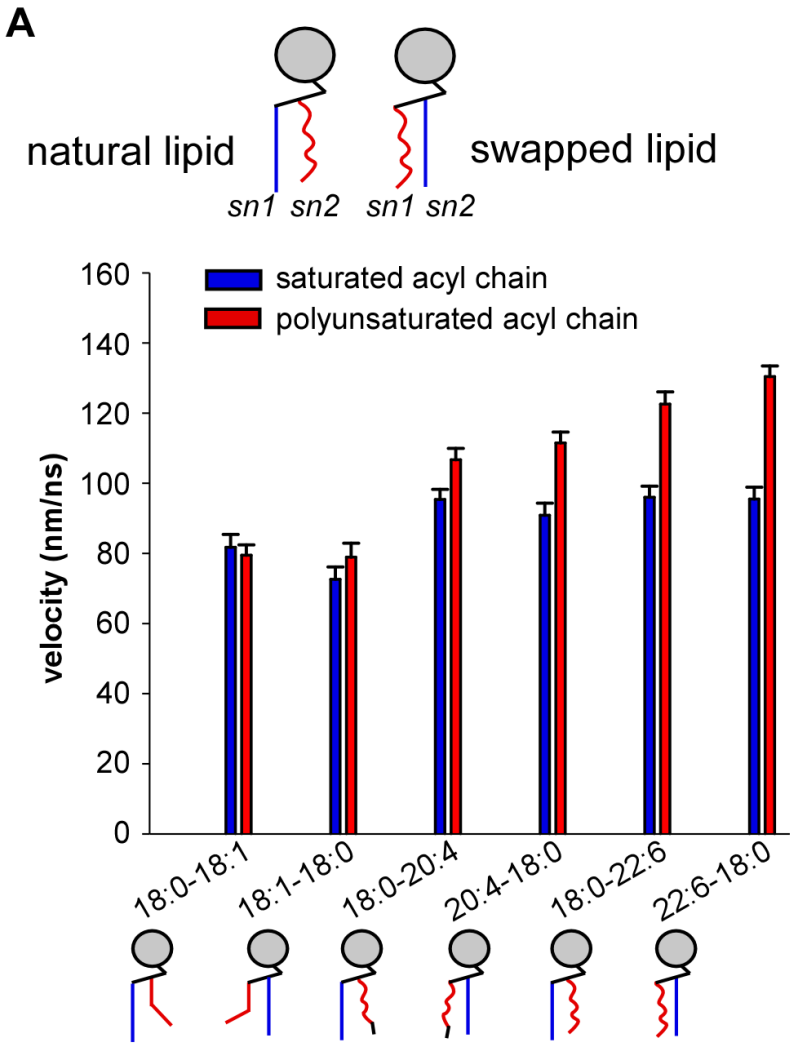


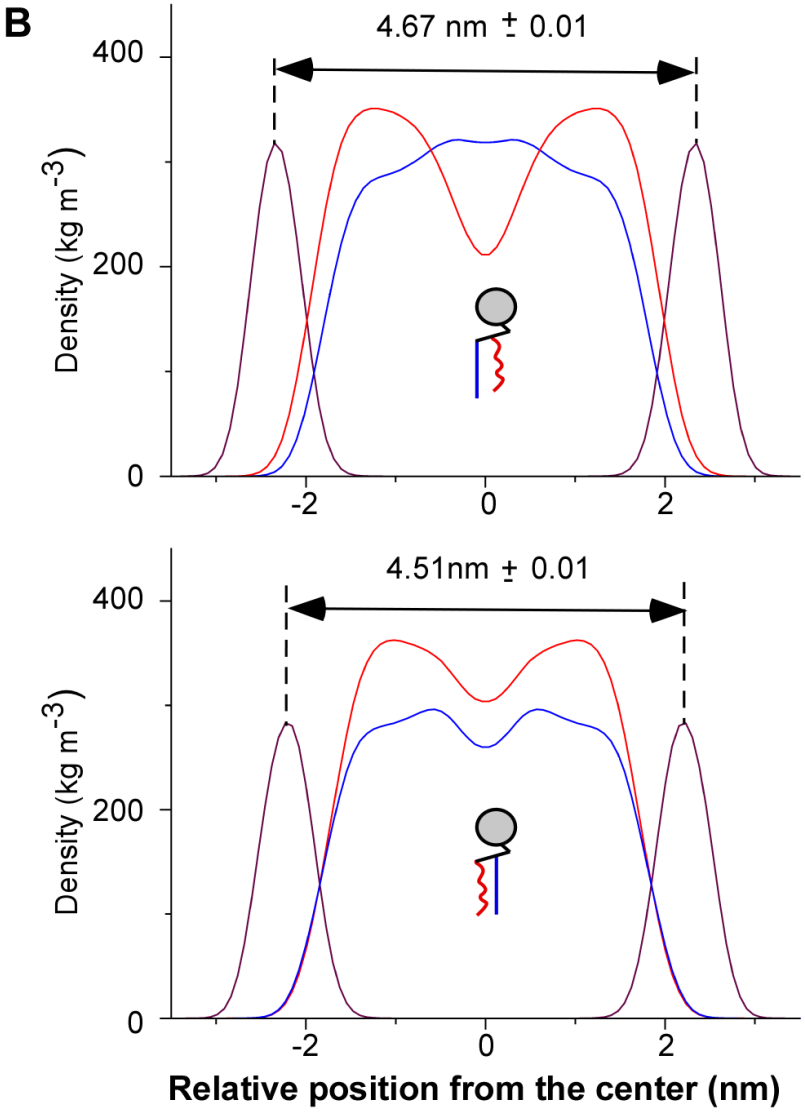


C

| Force KJ mol$^{-1}$ nm$^{-1}$ | pN | ~18:0-18:1 | ~18:1-18:0 | ~18:0-20:4 | ~20:4-18:0 | ~18:0-22:6 | ~22:6-18:0 |
|---|---|---|---|---|---|---|---|
| 175 | 290 | x x | x x | x x | x x | x x | x x |
| 200 | 332 | x x | x x | x x | F(109ns) F(127ns) F(134ns) | x x | F(93ns) F(68ns) F(177ns) |
| 230 | 382 | x x | x x | x x | F(52ns) F(42ns) | B(101ns) F(143ns) | F(38ns) F(43ns) |

X = Elongation
F = Fission
B = Breakage